

**CHARACTERIZATION AND PERFORMANCE EVALUATION OF
METAL ORGANIC FRAMEWORK FOR CARBON DIOXIDE GAS
ADSORPTION**

HO PUI SAN


**A project report submitted in partial fulfilment of the
requirements for the award of Bachelor of Engineering
(Honours) Chemical Engineering**

**Lee Kong Chian Faculty of Engineering and Science
Universiti Tunku Abdul Rahman**

April 2020

DECLARATION

I hereby declare that this project report is based on my original work except for citations and quotations which have been duly acknowledged. I also declare that it has not been previously and concurrently submitted for any other degree or award at UTAR or other institutions.

Signature :  _____

Name : Ho Pui San _____

ID No. : 16UEB01927 _____

Date : 18/5/2020 _____

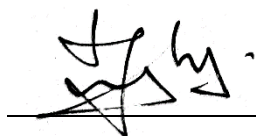
APPROVAL FOR SUBMISSION

I certify that this project report entitled “**CHARACTERIZATION AND PERFORMANCE EVALUATION OF METAL ORGANIC FRAMEWORK FOR CARBON DIOXIDE GAS ADSORPTION**” was prepared by **HO PUI SAN** has met the required standard for submission in partial fulfilment of the requirements for the award of Bachelor of Engineering (Honours) Chemical Engineering at Universiti Tunku Abdul Rahman.

Approved by,

Signature :

:



Supervisor :

:

Ir. Chong Kok Chung

Date :

:

18.05.2020

Signature :

:

Co-Supervisor :

:

Date :

:

The copyright of this report belongs to the author under the terms of the copyright Act 1987 as qualified by Intellectual Property Policy of Universiti Tunku Abdul Rahman. Due acknowledgement shall always be made of the use of any material contained in, or derived from, this report.

© 2020, Ho Pui San. All right reserved.

ACKNOWLEDGEMENTS

I would like to thank everyone who had contributed to the successful completion of this project. I would like to express my gratitude to my research supervisor, Ir. Chong Kok Chung for his invaluable advice, guidance and his enormous patience throughout the development of the research.

In addition, I would like to express my gratitude to all the lab officers that have assisted and guided me throughout my research. I had been blessed with my friends and family for giving me encouragement and caring all the times.

ABSTRACT

Concerns about the global warming issue have directed to substantial interest in removing the carbon dioxide (CO₂) gas from flue gas or atmosphere. CO₂ sequestration with selective adsorption is an effective established carbon dioxide gas removal approaches due to its easy operation, low energy requirement and tunable selectivity. A new type of nano-porous materials known as metal-organic frameworks (MOF), which has gas adsorption capability with unprecedented high porosity and high loading capacity is developed as a new promising candidate for CO₂ gas capture. In this study, MIL-101 (Cr) MOF samples were fabricated under different crystallization time and loading of organic acid using chromium (III) nitrate nonahydrate (Cr(NO₃)₃·9H₂O) and benzene-1,4-dicarboxylic acid (BDC) while UiO-66 (Ce) MOF samples were synthesized under different loading of organic acid and modulator using cerium ammonium nitrate (CAN) and benzene-1,4-dicarboxylic acid (BDC). Both types of MOF samples will be fabricated by using solvent-free method (mechanochemical). The XRD results indicated that the fabricated MIL-101 (Cr) MOFs were well agreed with the literature studies with the similar 2θ peak observed in the analysis. The morphology of the MIL-101 (Cr) MOF with the Cr/BDC molar ratio of 1 to 1 and crystallization time of 4 hours (MIL-101(Cr)-1-4) captured by SEM illustrated the dispersion of small irregular granular shaped particles. The EDX analysis result revealed that the Cr element was successfully incorporated into all the fabricated MIL-101 (Cr) MOF in regardless of the ratio of Cr to BDC and crystallization time. Carboxylic organic linker that participated the reaction was the source for the existence of C atom and O atom within the samples. The FTIR spectra of the synthesized MIL-101 (Cr) MOFs suggested the spectrum are well corresponding with that reported in the literature, especially for the fingerprint region. Hence, this confirming the formation of MIL-101(Cr) MOF. An intense absorption band was observed at 1390cm⁻¹ due to symmetric (O-C-O) vibration of the benzene ring. While the moderate intensity of absorption band observed at wavenumber of 720 cm⁻¹ is attributed to mono-substituted benzene ring. The CO₂ gas adsorption result exhibited that the MIL-101(Cr)-1-4 yield the highest adsorption capacity at 18.7772 mmol/g, suggested that the MIL-101(Cr) sample with

the Cr/BDC molar ratio of 1:1 and crystallization time of 4 hours exhibits good CO₂ gas adsorption performance.

TABLE OF CONTENTS

DECLARATION		i
APPROVAL FOR SUBMISSION		ii
ACKNOWLEDGEMENTS		iv
ABSTRACT		v
TABLE OF CONTENTS		vii
LIST OF TABLES		x
LIST OF FIGURES		xi
LIST OF SYMBOLS / ABBREVIATIONS		xv
 CHAPTER		
1	INTRODUCTION	1
1.1	Emission Sources of Carbon Dioxide (<i>CO</i> ₂) Gas	1
1.2	Global Warming and Its Effect	4
1.3	Importance of the Study	5
1.4	Introduction of Metal-Organic Framework (MOF)	6
1.5	Problem Statement	7
1.6	Aims and Objectives	7
1.7	Scope and Limitation of the Study	8
2	LITERATURE REVIEW	10
2.1	Atmospheric Carbon Dioxide Gas Removal Methods	10
2.1.1	Reforestation	10
2.1.2	Enhanced Weathering	10
2.1.3	Carbon Capture and Sequestration (CCS)	10
2.2	CO ₂ Separation Technologies	12
2.2.1	Membrane Separation	12
2.2.2	Cryogenic Separation	13
2.2.3	Liquid Scrubbing	13
2.2.4	Adsorption/Desorption	13
2.3	Overview of MOF	14
2.4	Applications of MOF	17
2.4.1	Gas Storage Application	17

	2.4.2	Biomedical Application	18
	2.4.3	Catalytic Application	18
	2.4.4	Electrochemical Application	19
2.5		Important Parameters Affecting Structure of MOF	20
	2.5.1	Effect of Solvents	20
	2.5.2	Effect of pH	22
	2.5.3	Effect of Temperature	22
	2.5.4	Effect of Crystallization Time	24
	2.5.5	Effect of Molar Ratio of Starting Materials	25
2.6		MOF Synthesis Methods	26
	2.6.1	Hydrothermal/Solvothermal Method	27
	2.6.2	Microwave-assisted Method	28
	2.6.3	Sonochemical Method	29
	2.6.4	Electrochemical Method	30
	2.6.5	Mechanochemical Method	31
2.7		Properties of MOFs in Carbon Dioxide Gas Adsorption	32
	2.7.1	Capacity for CO ₂	32
	2.7.2	Selectivity for CO ₂	32
	2.7.3	Coordinatively Unsaturated Metal Sites	33
	2.7.4	Enthalpy of Adsorption	34
2.8		Characterization Techniques and Instrumentations	34
	2.8.1	Scanning Electron Microscope Coupled with Energy-Dispersive X-ray Spectrometer (SEM-EDX)	35
	2.8.2	X-ray Diffractometer (XRD)	36
	2.8.3	Fourier-Transform Infrared Spectrometer (FTIR)	37
	2.8.4	Thermal Gravimetric Analyzer (TGA)	38
2.9		MIL-101 (Cr) MOF	38
2.10		UiO-66 (Ce) MOF	40
3		METHODOLOGY AND WORK PLAN	42
	3.1	Materials and Chemicals Used for MOFs Synthesis	42
	3.1.1	Materials and Chemicals for the Preparation of MIL-101(Cr)	42

3.1.2	Materials and Chemicals for the Preparation of UiO-66(Ce)	42
3.2	Preparation of Metal-Organic Frameworks	42
3.2.1	Preparation of MIL-101(Cr) MOF	42
3.2.2	Preparation of UiO-66(Ce) MOF	43
3.3	Parameters Study	45
3.3.1	Parameters Study of MIL-101(Cr) MOF	45
3.3.2	Parameters Study of UiO-66(Ce) MOF	45
3.4	Characterization Techniques and Instrumentations	46
3.4.1	Scanning Electron Microscope Coupled with Energy-Dispersive X-ray Spectrometer (SEM-EDX)	46
3.4.2	X-ray Diffractometer (XRD)	47
3.4.3	Fourier-Transform Infrared Spectrometer (FTIR)	47
3.5	Carbon Dioxide (CO ₂) Gas Adsorption Test	48
4	RESULTS AND DISCUSSION	50
4.1	Morphological Studies	50
4.1.1	For MIL-101(Cr) Study	50
4.1.2	For UiO-66(Ce) Study	50
4.2	X-Rays Diffraction (XRD) Graphs	52
4.3	Scanning Electron Microscopy (SEM) Images	53
4.3.1	Study on Cr/BDC Molar Ratio	53
4.3.2	Study on Crystallization Time	57
4.4	Elemental Dispersive X-Rays (EDX) Results	58
4.5	FTIR Analysis	60
4.6	Results for Gas Adsorption Test	61
5	CONCLUSIONS AND RECOMMENDATIONS	64
5.1	Conclusions	64
5.2	Recommendations for future work	64
	REFERENCES	66

LIST OF TABLES

TABLE	TITLE	PAGE
2.1	Examples of MOFs Catalysed Reactions (Pettinari, et al., 2017).	19
4.1	Elemental Composition of MIL-101 (Cr) with Different Cr/BDC Molar Ratio.	59
4.2	Elemental Composition of MIL-101 (Cr) with Different Crystallization Time.	60
4.3	Carbon Dioxide Gas Adsorption Result for MIL-101 (Cr) Samples with Different Molar Ratio of Cr to BDC.	63

LIST OF FIGURES

FIGURE	TITLE	PAGE
1.1	Atmospheric CO ₂ Concentration Over Years (Roser, et al., 2019).	1
1.2	Natural Sources of Carbon Dioxide (Pachauri and Reisinger, 2007).	2
1.3	Human Sources of Carbon Dioxide Gas (Le Quéré, et al., 2013).	3
1.4	Greenhouse Effect.	4
1.5	Schematic Diagram of Metal Organic Framework (MOF) (Nanowerk, 2019).	6
2.1	Pre-Combustion Carbon Capture (Kenji.S, 2011).	11
2.2	Oxy-Fuel Combustion System (Kenji.S, 2011).	12
2.3	Post-Combustion Carbon Capture (Kenji.S, 2011).	12
2.4	Geometries of Metal Ions and Organic Linkers (Kitagawa, Kitaura and Noro, 2004).	15
2.5	Illustration Dynamic Behaviours of 1,2 and 3-dimensional MOFs Structures When Reacting with Guest Molecules (Murdock, Lu and Jenkins, 2013).	16
2.6	MOFs' applications (Pettinari, et al., 2017).	17
2.7	(3){[Cd ₃ (BPT) ₂ (DMF) ₂ ·2H ₂ O}, (4) [Cd ₃ (BPT) ₂ (DMA) ₂] and (5) [(CH ₃ CH ₂) ₂ NH ₂]·{[Cd(BPT)]·2H ₂ O} formed by using Different Kinds of Solvents: DMF, DMA and DEF correspondingly (Li, et al., 2012 b).	21
2.8	Different Tm-succinates Compounds' Coordination Under Different Reaction Temperature, 100 °C and 180 °C (Carlos, et al., 2013).	24

2.9	Different Cu-Based MOF Coordination Structure Obtained Under Different Molar Ratio of Reactants (Luan, et al., 2006).	25
2.10	Different Zn-Based MOF Coordination Structure Obtained by Varying the Stoichiometry of Co-ligand (Wu, et al., 2011).	26
2.11	MOF Synthesis Methods and Their Respective Synthesis Conditions.	27
2.12	Schematic Diagram of Solvothermal Method (Lee, Kim and Ahn, 2013).	28
2.13	Schematic Diagram of Microwave-assisted Method (Lee, Kim and Ahn, 2013).	29
2.14	Schematic Diagram of Sonochemical Method (Lee, Kim and Ahn, 2013).	30
2.15	Schematic Diagram of Electrochemical Method (Lee, Kim and Ahn, 2013).	30
2.16	Schematic Diagram of Mechanochemical Method (Lee, Kim and Ahn, 2013).	32
2.17	Structure of Mg MOF 74 with Unsaturated Metal Sites Coordination (Trickett, et al., 2017).	34
2.18	Categories of Characterization Techniques.	35
2.19	Specimen Interaction in SEM.	36
2.20	Bragg's Law Diagram.	37
2.21	MIL-100 and MIL-101 Structural Frameworks (Bhattacharjee, et al., 2014).	39
2.22	Illustrations of Pentagonal Window and Hexagonal Window (Bhattacharjee, et al., 2014).	39
2.23	Schematic Diagram of Hydrothermal and Mechanochemical Synthetic Process of MIL-101 (Cr) MOF (Leng, et al., 2016).	40
2.24	Structural Framework of Ce-UiO-66 (Islamoglu, et al., 2017).	41

3.1	Flowchart for the Preparation of MIL-101(Cr) MOF.	43
3.2	Flowchart for the Preparation of Ce-UiO-66 MOF.	44
3.3	Hitachi S-3400N SEM-EDX Instrument.	46
3.4	Shimadzu Diffractometer 6000 model of XRD.	47
3.5	Nicolet iS10 FTIR Spectroscopy.	48
3.6	Gas Adsorption Test Setup.	49
3.7	Stainless Steel Closed Vessel (Blue Arrow Indicates the CO ₂ Gas Flow).	49
4.1	Colour Changes Along the Synthesis Process for MIL-101 (Cr).	50
4.2	Colour Changes Along the Synthesis Process for UiO-66 (Ce).	51
4.3	XRD Patterns of Various MIL-101 (Cr) Samples with (a) Different Cr/BDC Molar Ratio and (b) Different Crystallization Time.	52
4.4	XRD Patterns of Various MIL-101 (Cr) Samples in Literature Review (Leng, et al., 2016).	52
4.5	SEM Image for Pure Chromium Nanopowder (NANOSHEL, 2015).	54
4.6	SEM Micrographs of MIL-101(Cr)-2.5-4.	55
4.7	SEM Micrographs of MIL-101(Cr)-2-4.	55
4.8	SEM Micrographs of MIL-101(Cr)-1.5-4.	55
4.9	SEM Micrographs of MIL-101(Cr)-1-4.	56
4.10	SEM Micrographs of MIL-101(Cr)-0.5-4.	56
4.11	SEM Micrographs of MIL-101(Cr)-0.25-4.	56
4.12	SEM Micrographs of MIL-101(Cr)-0.2-4.	57
4.13	SEM Micrographs of MIL-101(Cr)-1-2.	57

4.14	SEM Micrographs of MIL-101(Cr)-1-4.	58
4.15	SEM Micrographs of MIL-101(Cr)-1-6.	58
4.16	SEM Micrographs of MIL-101(Cr)-1-8.	58
4.17	FTIR Spectra of Various MIL-101 (Cr) Samples with (a) Different Cr/BDC Molar Ratio and (b) Different Crystallization Time.	60
4.18	FTIR Spectra of Various MIL-101 (Cr) MOF samples (Leng, et al., 2016).	61
4.19	Carbon Dioxide Gas Adsorption Performance for MIL-101 (Cr) Samples with Different Molar Ratio of Cr to BDC.	63

LIST OF SYMBOLS / ABBREVIATIONS

CO ₂	carbon dioxide
H ₂ O	water vapour
N ₂ O	nitrous oxide
CH ₄	methane
O ₃	ozone
CFC	chlorofluorocarbon
MOF	metal organic framework
GHG	greenhouse gases
SO _x	sulfur oxide
NO _x	nitrogen oxide
CAN	cerium ammonium nitrate
BDC	1,4-benzene dicarboxylate
CCS	carbon capture and sequestration
RuBisCO	Ribulose-1,5-bisphosphate carboxylase/oxygenase
2-pymo	2-hydroxypyrimidinolate
sal	salicylaldehyde
PBP	1,4-bis[(3,5-dimethyl) pyrazol-4-yl]
tpha	tris(4-(1-(2-pyridin-2ylhydrazono) ethyl)-phenyl) amine
Li	Lithium
BTC	benzene-1,3,5-tricarboxylate
BTB	1,3,5-benzenetribenzoate
DEF	diethylformamide
DMF	dimethylformamide
DMSO	dimethyl sulfox
DMA	dimethylacetamide
BPYDC	2,2'-bipyridine-5,5'-dicarboxylate
H ₃ BPT	biphenyl tricarboxylic acid
HADA	1,3-adamantanediactic acid
2,4- PYDC	pyridine-2,4- dicarboxylic acid
H ₂ IIP	5-iodoisophthalic acid
bpp	1,3-bis(4-pyridyl) propane

hmaa	2-methylacrylic acid
H ₂ hfipbb	4, 4'- (hexafluoroisopropylidene) bis(benzoic acid)
dps	4, 4'-dipyridylsulfide
SFG	Solvent-free Grinding
LAG	Liquid-assisted Grinding
ILAG	Ion and Liquid Assisted Grinding
MIL	Material Institute Lavoisier
UiO	University of Oslo
SEM	Scanning Electron Microscope
EDX	Dispersive X-ray Spectrometer
XRD	X-ray Diffractometer
FTIR	Fourier-Transform Infrared Spectrometer
TGA	Thermal Gravimetric Analyzer
K	Kelvin
atm	atmospheric pressure
2,5-DOT	2,5-dioxidoterephthalate
M	Mg(ii), Zn(ii), Mn(ii), Fe(ii) and Ni(ii), among others
btz	5-bis(5-tetrazolo)-3-oxapentane
EtOH	ethanol
HF	hydrofluoric acid
Cr	chromium
Ce	cerium
Zr	zirconium

CHAPTER 1

INTRODUCTION

1.1 Emission Sources of Carbon Dioxide (CO_2) Gas

Generally, the carbon dioxide gas emission sources are from both induced natural and human. The human activities have caused the carbon dioxide concentration in atmosphere rising tremendously since the industrial revolution. The CO_2 concentration now has arrived at an alarming state. Although the human sources of emission are much smaller as compared to the natural sources, they have affected the natural balances that have existed for many thousands of years before the Industrial Revolution. The natural sinks have kept the atmospheric carbon dioxide level balanced by removing similar quantity of atmospheric CO_2 as that were producing by natural sources. However, the excessive CO_2 emission from the human activities have upset the natural balance of atmospheric CO_2 (What's Your Impact, 2018). The atmospheric CO_2 concentration has started to increase tremendously at 18th century, which is the start of Industrial Revolution (Figure 1.1).

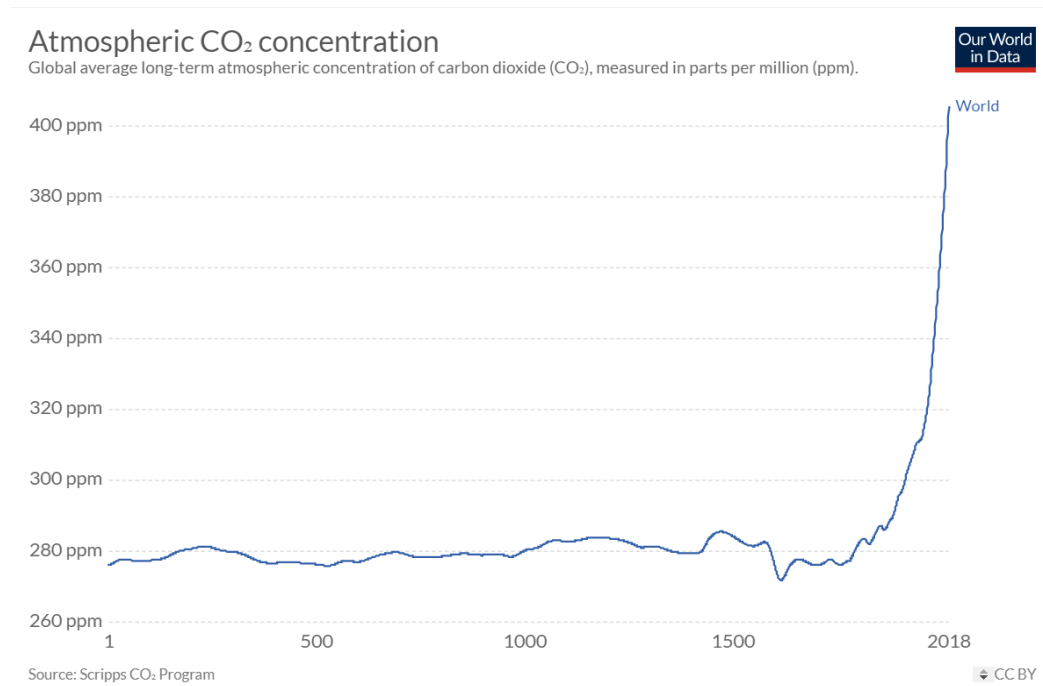


Figure 1.1: Atmospheric CO₂ Concentration Over Years (Roser, et al., 2019).

CO_2 will be released into atmosphere by natural processes, including ocean and atmosphere exchange, living things respiration process, volcanic eruptions, soil decomposition and etc. Ocean and atmosphere exchange are the largest natural source for CO_2 emission. Oceans contain dissolved CO_2 gas and release them into the atmosphere. This movement is in both direction and it happens at the sea surface. The second largest natural source for carbon dioxide gas emission is the respiration process of plants and animals, it accounts for about 30 % of the natural sources of atmospheric CO_2 (What's Your Impact, 2018).

Another important natural source for CO_2 gas emission is soil respiration and decomposition process. Decomposers likes bacteria and fungi make use of respiration process to produce energy that is needed for survival and emit CO_2 gas, this process is considered as soil respiration. These decomposers also break down the organic matter in soil and carbon dioxide is released during this decomposition process. Other than that, minor amount of CO_2 , about 0.15 - 0.26 billion tonnes of CO_2 is produced by volcanic eruptions every year (What's Your Impact, 2018).

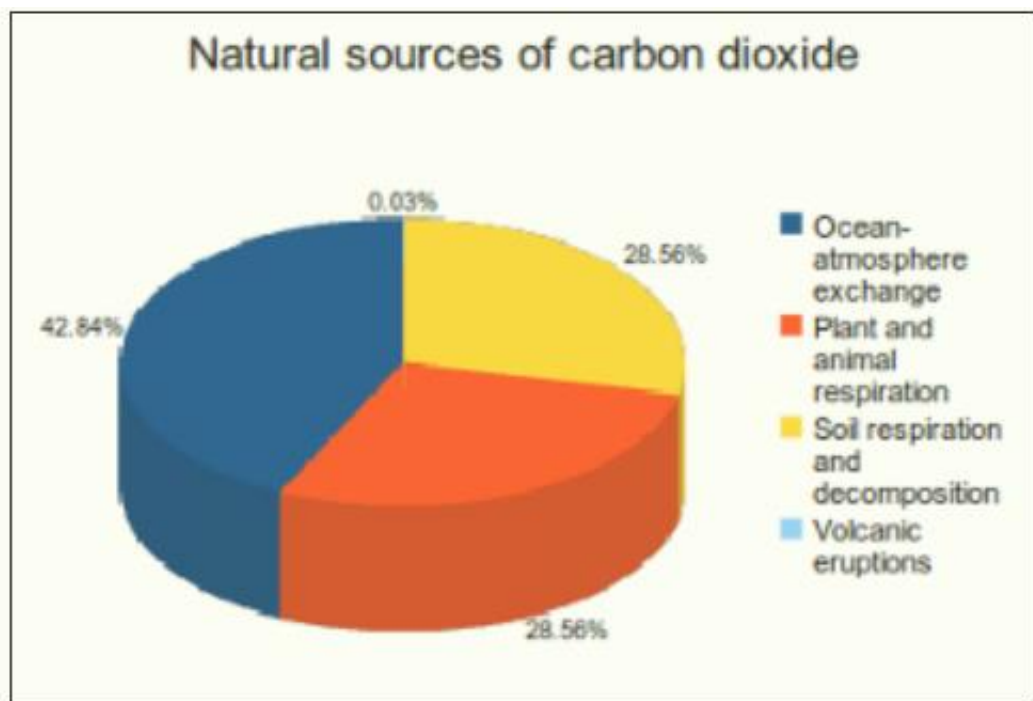


Figure 1.2: Natural Sources of Carbon Dioxide (Pachauri and Reisinger, 2007).

Burning of fossil fuel, industrial processes and logging activity, these human activities are the three main causes for the increased atmospheric carbon dioxide

concentration. Among of them, combustion of fossil fuel has accounted for 87 % of human sources of carbon dioxide gas, which is the largest human sources for CO_2 gas emission. The purpose of burning these fossil fuels is to turn the energy released during the burning process into heat, electricity or transportation power. The three main kinds of fossil fuels are natural gas, coal and oil. Among of them, coal is the most carbon intensive fossil fuel. In other words, burning coal will release the largest amount of CO_2 , approximately 2.5 tons of CO_2 are released into the atmosphere for every ton of coal was being burned (What's Your Impact, 2018).

Changes in land use has accounted for 9% of total human sources of carbon dioxide gas emission. Changes in land use are happened when the natural environment is changed into agricultural land or human settlement areas. Trees play a vital role as natural carbon sinks since they remove the atmospheric CO_2 by undergoing photosynthesis process. When the forests are cleared for human activities purpose, trees are being chopped down or either being burned, which further release CO_2 gas into air. Another 4% of human sources of carbon dioxide comes from industrial activities. Many industrial activities will produce significant amount of CO_2 gas as the by-products, and directly release them into the atmosphere.

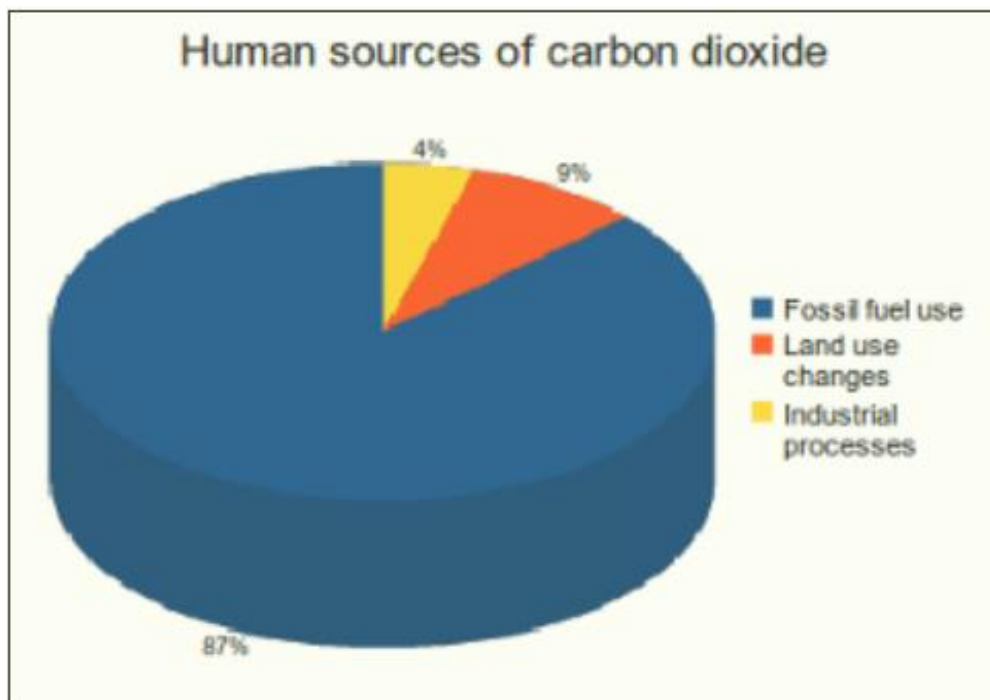


Figure 1.3: Human Sources of Carbon Dioxide Gas (Le Quéré, et al., 2013).

CO_2 is known as one of the greenhouse gases. Greenhouse gases will absorb and emit thermal radiation, creating the “greenhouse effect”, this effect can maintain our planet temperature at a habitable level (Roser, Hannah and Max, 2019). However, since the industrial revolution, human activities have increased the atmospheric CO_2 concentration rapidly and have upset the natural balances. Thus, the global carbon cycle has been disrupted and leading to a globally warming.

1.2 Global Warming and Its Effect

Scientists attribute the global warming trend observation since the mid-20th century to the human activities that causing the expansion of greenhouse effect. When the sun radiation reaches the Earth surface, part of the heat radiation is reflected back to space while another part of it will be absorbed by the atmosphere. This absorbed infrared radiation will be emitted from the Earth surface or be captured and reflected in all paths by greenhouse gas particles to warm the atmosphere and Earth surface (Figure 1.4).

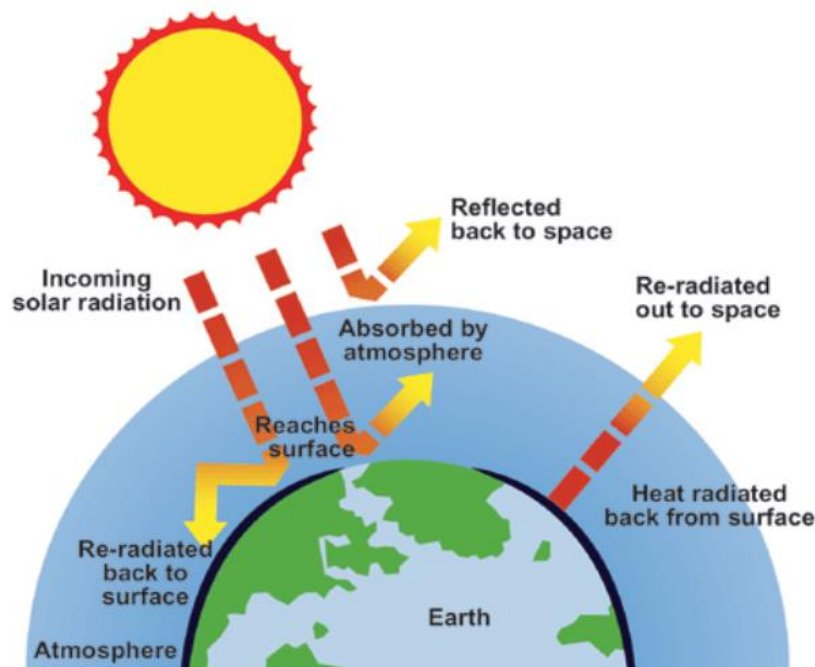


Figure 1.4: Greenhouse Effect.

Global warming, the increasing of overall atmospheric temperature is happened due to the greenhouse effect that caused by increment levels of carbon dioxide and other greenhouse gases, such as nitrous oxide (N_2O), water vapour

(H_2O), ozone (O_3), methane (CH_4) and chlorofluorocarbon (CFC). Among of them, CO_2 is the most important long-lived driving force for climate change since it responsible for about 60 % of the greenhouse effect. The CO_2 heat-trapping nature can disturb the transmission of infrared radiation through the air. It led to the increased levels of greenhouse gases, particularly the CO_2 will result in warmer Earth (NASA's Jet Propulsion Laboratory, 2019).

Literature study by NASA (NASA's Jet Propulsion Laboratory, 2019) shows that the average temperature of Earth surface has ascended about 0.9 °C since Industrial Revolution had started at late 19th century. The seas have captured much of this trapped heat and thus result in a rising of the ocean temperature of about 0.4 °F since 1969. Additionally, the mass of Antarctic and Greenland ice sheets declined tremendously every year from 1993 until 2006, they had lost approximately 127 billion and 286 billion tons of ice correspondingly. All these facts have proven that the human sources of carbon dioxide gas emission are the main driving force for the global warming phenomenon.

Scientists anticipated that the worldwide temperature would remain rising in the coming decades, largely due to the greenhouse gases that are emitted from human activities. The global temperature is forecasted to be risen between 2.5 to 10 °F in the coming hundred year (NASA's Jet Propulsion Laboratory, 2019). Rising temperature will not only affect wildlife and their habitats. The global sea level is also expected to rise another 1 – 4 feet by 2100 (NASA's Jet Propulsion Laboratory, 2019), in which will flood the low-lying areas. Besides that, more droughts and heat waves will occur and thus increase the risk of wildfires, drinking water shortages and lost crops.

1.3 Importance of the Study

The sections above have outlined that the human sources of CO_2 gas have led to the atmospheric carbon dioxide concentration reaching an unhealthy level in which will cause greenhouse effect and drive the global warming issue to a more serious stage. There are many serious negative impacts that would be brought by the global warming as discussed in the section above, including increment of sea level, more drought, extreme weather conditions and etc.

Therefore, there is a need to carry out the study regarding to physical removal of atmospheric CO_2 gas and my study will be focused on using new type of material,

Metal-Organic Frameworks (MOFs) to adsorb the excessive atmospheric CO_2 gas in order to achieve environment carbon balance for sustainable development.

1.4 Introduction of Metal-Organic Framework (MOF)

MOF is a combination of organic and inorganic hybrid crystalline porous material. Its systematic arrangement is that the collection of positively charged metal ions, surrounded with organic linker molecules (Nanowerk, 2019). The metal atoms form intersections that tie the organic ligands jointly to assemble a cage-like arrangement, which is shown in the schematic diagram below.

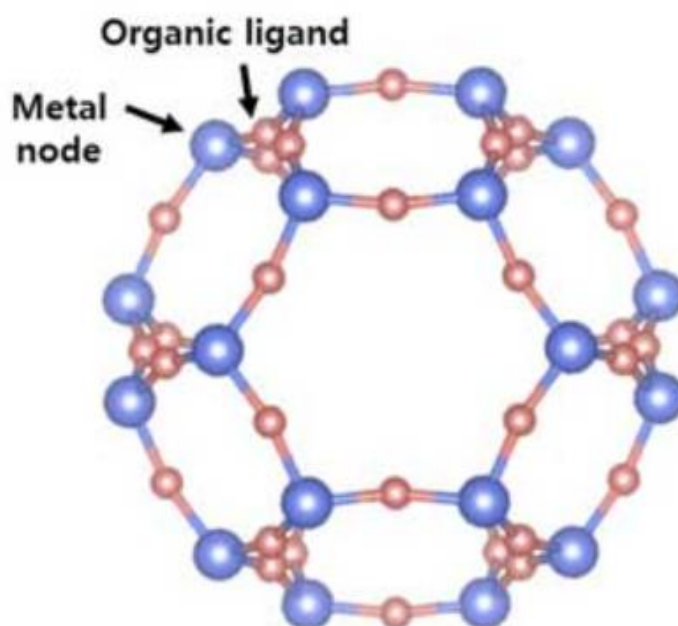


Figure 1.5: Schematic Diagram of Metal Organic Framework (MOF) (Nanowerk, 2019).

MOF has an extraordinarily huge internal surface area. Up until now, the largest surface area of MOF that is able to be synthesized by researchers can go up to $7,000 \text{ m}^2/\text{g}$. It is a crystalline nanoporous material that is consisting of both organic and inorganic molecules in a firm framework. Thus, it offers unique structural diversity: uniform pore structures and atomic-level structure while flexible in network topology, porosity and chemical functions. MOFs with different structures are possible to be produced by varying the combinations of metal precursors and organic ligands. A range of kinetic and thermodynamics will form different

structures of MOFs as well. Hollow structure of MOF has provided it with wide variety of advantageous features, including high surface area, high porosity, low density and high loading capacity (Nanowerk, 2019).

The first journal on MOF was written by Prof. Omar Yaghi and published in the late 1990s, “Design and synthesis of an exceptionally stable and highly porous metal-organic framework” (Nanowerk, 2019). Soon after that, MOFs have becoming a rapid growing research field in the academia. Up until today, over 20,000 distinct kinds of MOFs have been successfully fabricated and identified (Nanowerk, 2019).

Applications of MOFs in numerous fields are being developed due to its unprecedented porosity with periodical and versatile chemistries, they are including catalysis, sensing, electrochemical energy storage, liquid purification, gas capture etc. These applications are mostly based on catalysis, storage and separation characteristics.

1.5 Problem Statement

Concerns about the global warming issue have directed to substantial interest in removing the CO₂ gas from flue gas or atmosphere. CO₂ sequestration with selective adsorption is an effective established carbon dioxide gas removal approaches due to its easy operation, low energy requirement and tunable selectivity. Zeolites, carbon-based materials, inorganic molecular sieves and many other materials have been investigated for CO₂ gas adsorption.

However, a new type of nanoporous material, Metal-Organic Framework, which has gas adsorption capability with unprecedented high porosity and high loading capacity is developed. Different combinations organic linkers and metal oxides or ions will self-assemble to make up many types of MOFs with uniform pores, great surface areas, versatile in chemical functions and structures. These attractive features have enabled MOFs as a new promising candidate for CO₂ gas capture.

1.6 Aims and Objectives

The purpose for this research study is to study the parameters that would affect the CO₂ gas adsorption performance of MOFs (MIL-101 (Cr) and UiO-66 (Ce)). The objectives of the research are outlined as:

- (i) To study the effect of fabrication parameters (molar ratio of metal ions to organic ligand, crystallization time and the addition of acetic acid as modulator) on the behavioural changes of MOFs.
- (ii) To investigate the chemical and physical properties of MOF by characterization study.
- (iii) To examine the CO_2 gas adsorption performance on the self-fabricated MOFs.

1.7 Scope and Limitation of the Study

In this study, two types of MOFs: MIL-101 (Cr) and UiO-66 (Ce) were fabricated by utilizing solvent-free method (mechanochemical). The fabricated MOFs were then be tested on CO_2 gas adsorption performance. Apart from the CO_2 gas adsorption test, the samples were analysed by using some characterization equipment, they are including XRD, SEM-EDX, FTIR and TGA to study their chemical and physical properties in relation to their properties of CO_2 gas adsorption.

For MIL-101 (Cr) MOF study, it can be divided into two parts. The first part of the study is to investigate the effect of molar ratio between Cr metal ion and BDC organic ligand on its CO_2 gas adsorption performance, the later part is to manipulate the crystallization time of the chosen molar ratio to determine the most appropriate fabrication condition for the MIL-101 (Cr) MOF.

While for the study of Ce-UiO-66 MOF, the molar ratio between cerium ammonium nitrate (CAN) and organic ligand (BDC) is manipulated. Apart from that, a series of samples are synthesized by adding acetic acid as modulator and another set of samples without acetic acid to investigate its effect on the adsorption property.

The main limitation for this study is the structure prediction of MOF. Different coordination linkages and geometries are possible for MOF synthesis, thus making the formation of MOF with the desired structure during the synthesis become challenging. Normally, only a narrow and specific set of reaction condition would make the synthesis of the corresponding MOF successful. Besides that, long reaction time in conjunction with expensive reactants also restrict the synthesis of MOFs.

Although the Ce-UiO-66 MOF samples have been successfully fabricated, the characterization tests and the carbon dioxide gas adsorption test for these samples were unable to be conducted as planned due to the implementation of Movement Control Order (MCO) in Malaysia. Hence, it had greatly affected the study work of

fabrication parameters in relation to carbon dioxide gas adsorption performance for Ce-UiO-66 type of MOF samples.

CHAPTER 2

LITERATURE REVIEW

2.1 Atmospheric Carbon Dioxide Gas Removal Methods

It is not only necessary to keep the emission of carbon dioxide at low level, but also a must to remove and store some carbon from the atmosphere in order to maintain the global temperature rise to less than 1.5 °C. Atmospheric carbon dioxide gas removal can be in a number of forms: reforestation, enhanced weathering, and the most widely applied method, carbon capture and sequestration method.

2.1.1 Reforestation

The most natural way of removing the atmospheric carbon dioxide gas is by expanding the forests and restoring the existing forests. Trees can naturally store carbon and remove it from atmosphere by photosynthesis. This approach can be relatively inexpensive and result in cleaner air and water (Mulligan, Ellison and Levin, 2018). However, reforestation would reduce the food supply and land use for other activities. Furthermore, it is a less efficient approach for removing carbon dioxide gas as compared to other available methods.

2.1.2 Enhanced Weathering

Another potential method for carbon removal in atmosphere is enhanced weathering. Weathering refers to a process when some minerals naturally reacts with CO_2 , converting carbon from carbon dioxide gas into a solid. However, this reaction typically happens at extremely slow rate. But scientists are finding ways to speed up this process, especially by enhancing the exposure of these minerals to CO_2 gas that exists in the air or ocean. Scientists have shown that this approach is possible, but more research works have to be done to find out the most cost-effective and efficient applications of this approach (Mulligan, Ellison and Levin, 2018).

2.1.3 Carbon Capture and Sequestration (CCS)

It is broadly recognized as a major approach eliminating the amount of atmospheric CO_2 , which is commonly attached with coal-fired power plants. It is a combined approach that comprising of three stages: CO_2 is captured from industrial flue gas;

afterwards, the captured CO_2 is transported to a storage site and subsequently will be stored underground in depleted oil and gas fields. There are total three main kinds of existing carbon capture processes for CCS: pre-combustion, oxyfuel and post-combustion (Coninck, Stephens and Metz, 2009). They are distinct in the first stage of carbon capture process, but for the following stages of transportation and storage process they are basically the same.

The inlet fuel is transferred into a mixture of hydrogen gas and carbon dioxide gas in the pre-combustion system before undergoing combustion process. After that, the CO_2 gas is separated out and sent to compression unit for underground storage while hydrogen gas is further used as input fuel for undergoing combustion process for electricity production. The overview of the pre-combustion for carbon capture process is illustrated in the Figure 2.1.

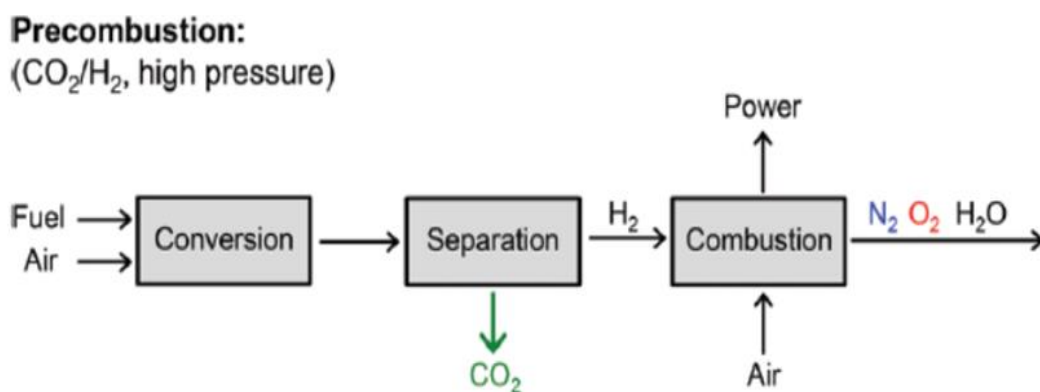


Figure 2.1: Pre-Combustion Carbon Capture (Kenji.S, 2011).

Oxy-fuel combustion requires the separation of nitrogen gas from the air mixture prior to combustion process (Figure 2.2). Thus, the inlet fuel will be combusted under oxygen-rich environment instead of in air. This combustion condition will result in flue gas containing mainly CO_2 and H_2O . A more concentrated CO_2 stream of flue gas is easier for later purification process.

Oxy-Fuel Combustion:
(O_2/N_2 , low pressure)

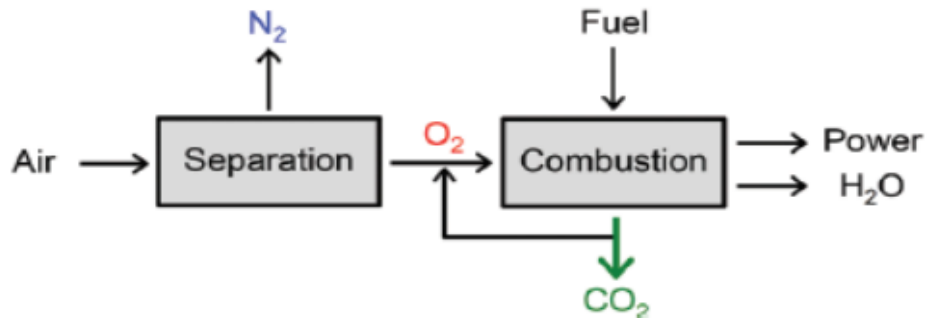


Figure 2.2: Oxy-Fuel Combustion System (Kenji.S, 2011).

For the post-combustion carbon capture process, the CO_2 will only be separated out after the combustion process (Figure 2.3). There are several separation technologies offered for separating out the CO_2 , including membrane filtration, cryogenic separation, liquid scrubbing and adsorption/desorption.

Postcombustion:
(CO_2/N_2 , low pressure)

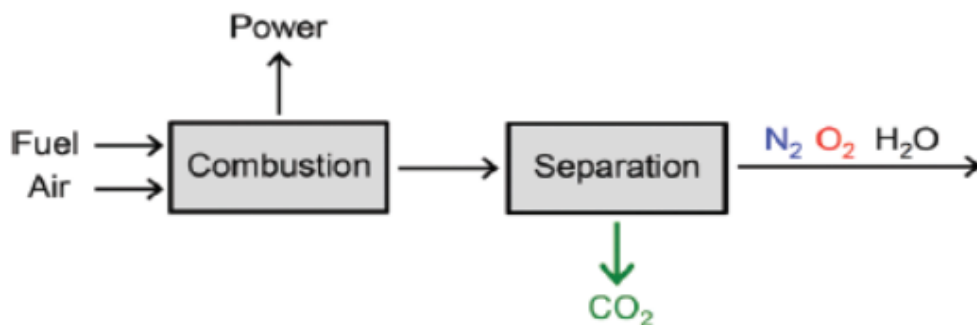


Figure 2.3: Post-Combustion Carbon Capture (Kenji.S, 2011).

2.2 CO_2 Separation Technologies

Various separation technologies include of membrane separation, liquid scrubbing, cryogenic separation and adsorption will be discussed in detailed in the following subsections.

2.2.1 Membrane Separation

Membrane plays role as a semi-permeable barrier by only allowing relatively free passage of one component while attaining another in membrane separation process.

The advantageous feature for this separation process is that it is an inexpensive process for separating gas and it is able to maintain high product purity. However, its removal efficiency is relatively low and low concentration of CO_2 will make this separation process inefficient (Mondal, Balsora and Varshney, 2012).

2.2.2 Cryogenic Separation

Cryogenic separation happens at a temperature that is below the material freezing point. Under this temperature, materials will become brittle and subsequently can easily be separated by impact. Cryogenic separation process only suitable for separation of CO_2 from the stream that is having high CO_2 concentration, which is typically more than 50 %. No chemical adsorbent is needed in this separation process and it can be conducted at atmospheric pressure. However, this separation technique is unsuitable for the stream that is containing other gases except carbon dioxide, such as SO_x , NO_x and H_2O , since these gases will affect the cooling process and many problems including the erosion, fouling and plugging will arise (Mondal, Balsora and Varshney, 2012).

2.2.3 Liquid Scrubbing

Liquid scrubbing is founded on the reaction between CO_2 and chemical solvent. When CO_2 gas contacting with a liquid, it will be absorbed into the solvent liquid (Mondal, Balsora and Varshney, 2012). Merit for this separation process is that it can handle with bulk amount of CO_2 stream with the separation efficiency up to about 90 %. On the other hand, its drawbacks are corrosion problem, high energy consumption and degradation of the absorbent (Dinda, 2013).

2.2.4 Adsorption/Desorption

Adsorption process happens when one or more elements of a fluid stream is being captured on the surface of solid adsorbent. In the case of CO_2 capture, a stream containing CO_2 gas will be passed through the solid adsorbent bed and CO_2 gas as the targeted gas component will be separated out. Advantages for this adsorption separation process are low operating cost, low energy requirements and high removal efficiency of about 90 % while its main disadvantage is the complexity of process configuration (Kaithwas, Prasad and Verma, 2012).

Zhao (2012) proposed that among of these separation methods, adsorption process appeared to be the most promising choice owing to its low operating and apparatus cost, low energy consumption and easy to apply. Numerous materials including zeolites and activated carbons are potential solid adsorbents for carbon dioxide gas separation. Among of them, activated carbon is the most generally applied and efficient solid adsorbent due to its large surface area and porosity. Nevertheless, the high cost of activated carbon has limited its application where researchers are finding alternative adsorbent which have lower cost and equivalent adsorption efficiency.

2.3 Overview of MOF

MOF also known as metal-ligand coordination polymer, is a combination of organic and inorganic hybrid stretched network formed through covalent bonding. Most of the metal ions are transition metals since they have versatile coordination numbers, and this could form lots of various geometries, including square planer, tetrahedron and octahedron. While for the organic linkers, they consist of cyanides, halides, anionic and organic molecules (Kitagawa, Kitaura and Noro, 2004). The constituent of MOF is shown in Figure 2.4. Subsequently, further to the metal ions/clusters and organic linker bonding together, MOF can form n-dimensional structures that show flexibility upon interacting with the guest molecules and its schematic diagram is demonstrated in Figure 2.5.

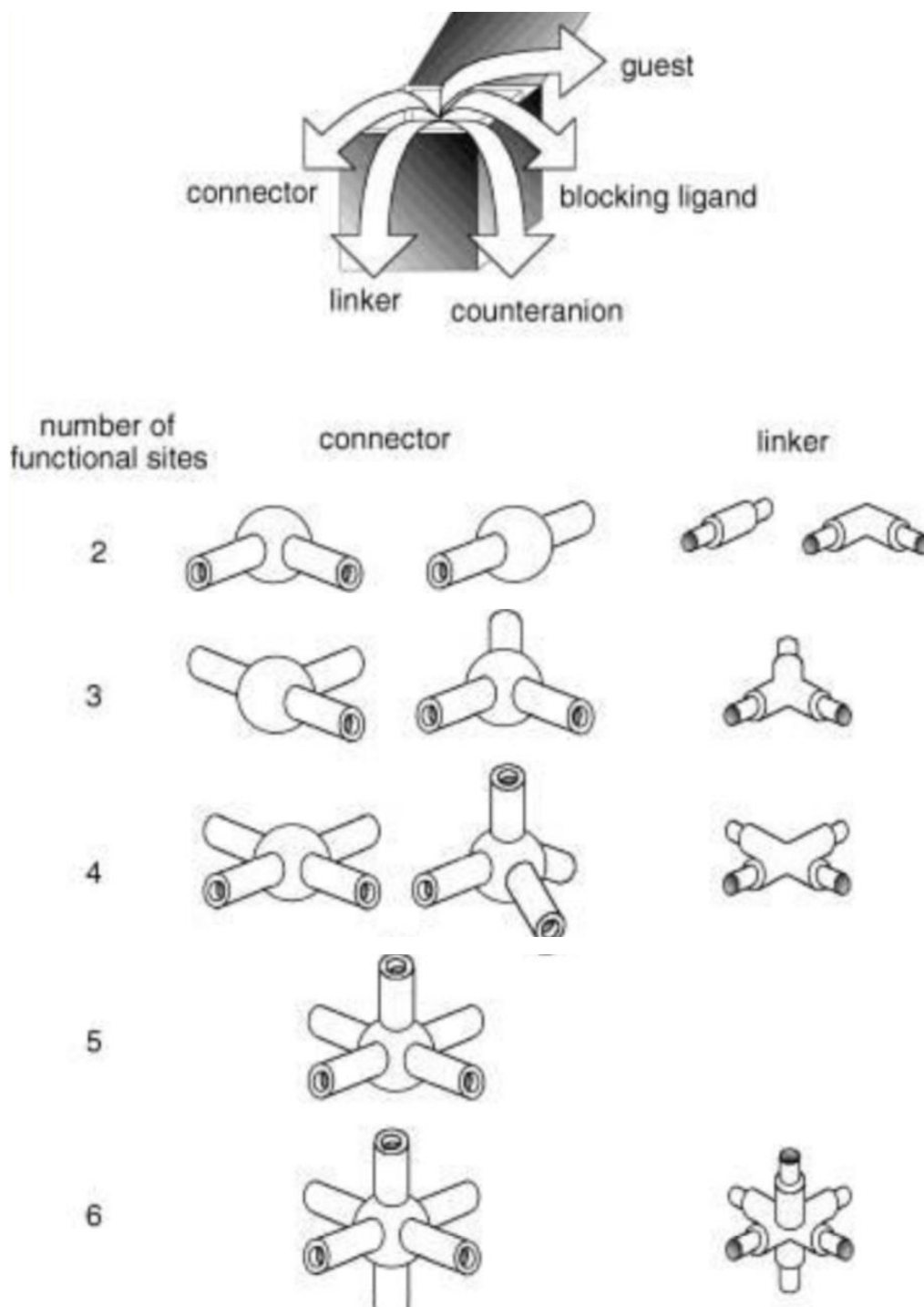


Figure 2.4: Geometries of Metal Ions and Organic Linkers (Kitagawa, Kitaura and Noro, 2004).

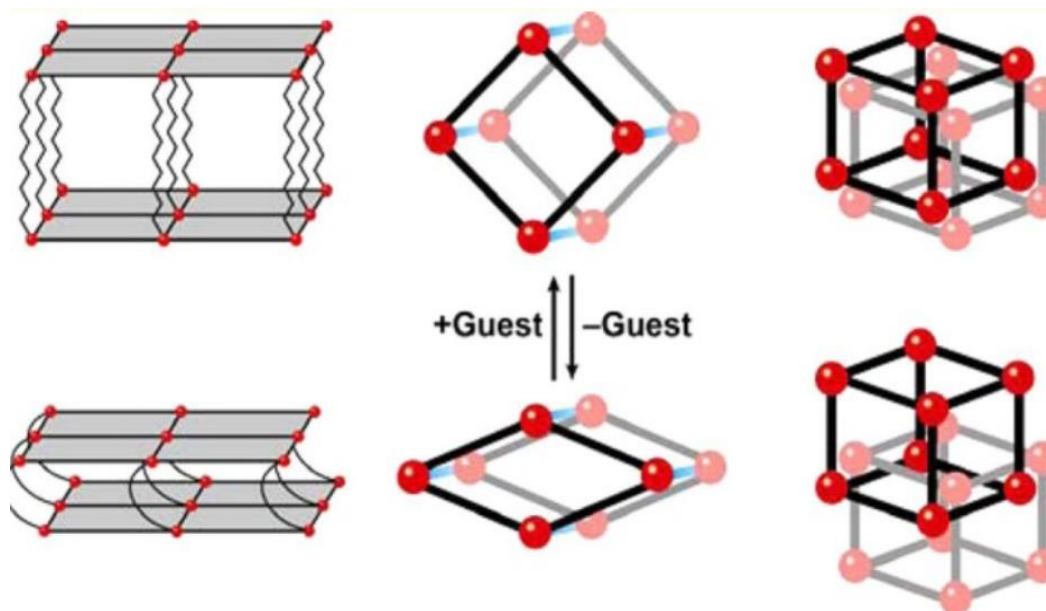


Figure 2.5: Illustration Dynamic Behaviours of 1,2 and 3-dimensional MOFs Structures When Reacting with Guest Molecules (Murdock, Lu and Jenkins, 2013).

MOF is a new type of nano-porous material. They tend to display unique properties depending on the incorporation of different kinds of components and the ways the components bond together. MOFs have three major distinct features, they are high surface area associated with high porosity, ordered and tuneable pore structure and flexibility in structure building.

Researchers have successfully created the MOF with specific surface area of greater than $7000 \text{ m}^2/\text{g}$, in which analogous to the surface area of a soccer field with a teaspoon of this material (Nanowerk, 2019). MOFs have pores that can be modified to fit into specific applications. Pores shapes and sizes are essential to ensure interactions between the host and guest atoms and these pore structures could be manipulated by changing the dimension of organic linkers. Furthermore, MOFs' flexible structure contrast to the rigid zeolite framework have enabled them to replace the zeolites in application of gas or liquid adsorption and catalytic activity. These distinct features have empowered MOFs superior performances and wide range of applications (Alhamami, Doan and Cheng, 2014).

2.4 Applications of MOF

The main features of MOFs, high porosity volume and large surface area has made them comparable to zeolites and even some of them have exceeded those in zeolites. MOFs with surface area more than seven thousand square meters per gram have been synthesized by researchers. Their great surface areas have made them possible to adsorb great amounts of different types of gases, like hydrogen, methane and carbon dioxide gas.

Besides that, MOFs' other features like small density, tunable porosity and structural flexibility also have made them useful in many applications, for example heterogenous catalysis, supercapacitors and sensing (Vieth, Janiak and Jana, 2010) (Figure 2.6).

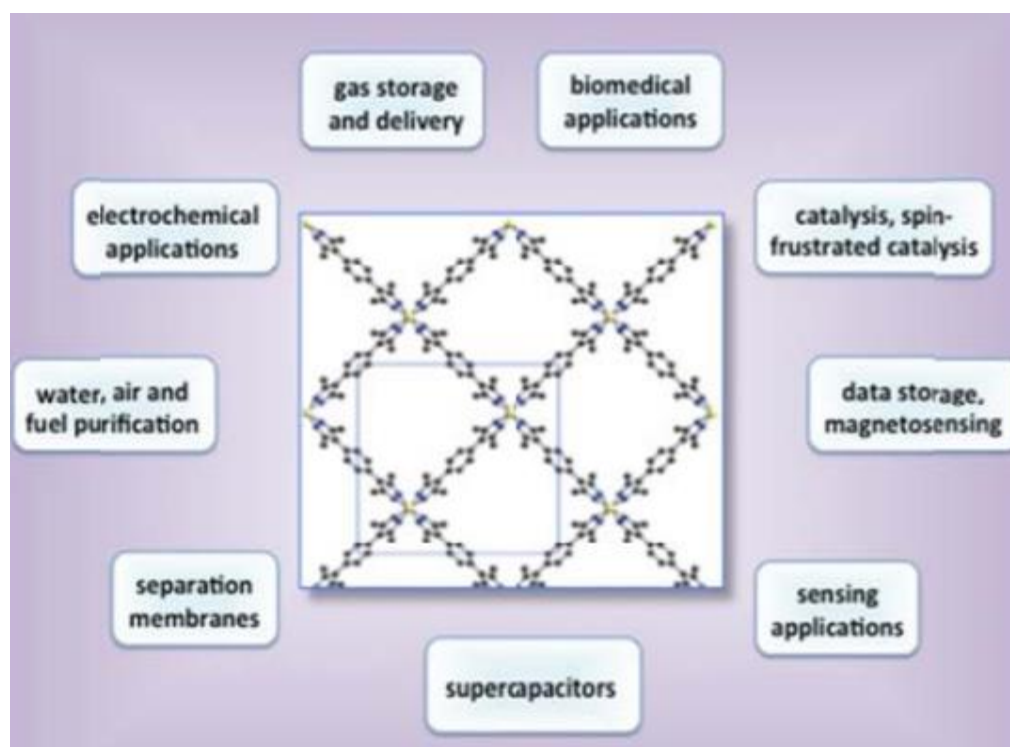


Figure 2.6: MOFs' applications (Pettinari, et al., 2017).

2.4.1 Gas Storage Application

MOFs' major application is gas adsorption owing to their extraordinarily large surface area. It is clean energy application for MOF as it is able to be applied in the gas capture and storage for hydrogen, methane and carbon dioxide gas. MOFs are supreme solid adsorbents for hydrogen gas storage, the most promising MOF can store high hydrogen gas densities up to 10% wt at temperature of 77 K (Zhao, Yuan

and Zhou, 2008). While the 3-D $[\text{Cu}(\mu\text{-SiF}_6)(4,4'\text{-byp})_2] \cdot 8\text{H}_2\text{O}$ at pressure above 5 bar can adsorb greater amount of methane gas than a zeolite (Noro, et al., 2000).

2.4.2 Biomedical Application

MOFs are potential material as drug deliverer since they can modify their properties by changing the functional groups of the frameworks or by fine-tuning the pore size. The MIL family, owing to their big pore sizes and great surface areas of about 3,100 to 5,900 m^2/g , it is a potential class of MOF for drug delivery purpose. Especially for the MIL-100 and MIL-101, they have distinct structure and uniform porosity, thus both of them have been utilized for the delivery of ibuprofen (Kızılel and Keskin, 2011).

Besides, several types of MOFs have been discovered that owning hydrophilic holes that carry charges, which are very suitable in encapsulating drugs that are carrying the opposite charges with regard to the MOFs. Furthermore, biomolecules and biocompatible metal cation can be incorporated into the MOFs' framework as linkers or nodes for imaging applications (McKinlay, et al., 2010)..

2.4.3 Catalytic Application

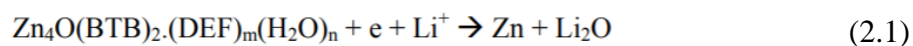
MOF is an alternative class of heterogeneous catalysts. The fabrication of MOFs characterized with local structure similar to that found on the catalysts that have the required catalytic activity could be done by sensibly choosing the type of organic linker and suitable design. MOF offers active sites where the molecules can be orientated while the transition state can be stabilized. Owing to the unsaturated metal centres or catalytic species that are present within the inherent sites or pores, MOFs possesses with good catalytic activity. Besides, MOF catalytic activity can also happen at the organic linker. Some of the selected MOF derived from literature studies and its catalysed reactions are tabulated in Table 2.1.

Table 2.1: Examples of MOFs Catalysed Reactions (Pettinari, et al., 2017).

MOF	Catalysed Reaction
Cu(2-pymo) ₂	Aerobic olefin oxidation
Co(sal)(H ₂ O)(py) ₃	Olefin epoxidation
[Cd(bpy) ₂](NO ₃) ₂	Cyanosilylation of aldehydes
MIL-100(Fe)	Friedel Crafts benzylation
ZIF-8	Cycloaddition of CO and epoxides
UiO-66	Cyclization of citronella
Co(PBP)	Olefin oxidation
[Ag ₃ (tpha) ₂](BF ₄)	1,3-dipolar cycloaddition
MIL-101(Cr)	Heck coupling/Knoevenagel condensation
Cu ₃ (btc) ₂	Isomerization
Zn ₄ O(bdc) ₃	Friedel-Crafts alkylation
Pd(2-pymo) ₂	Alcohol oxidation

2.4.4 Electrochemical Application

MOFs materials can be applied for lithium ion batteries as an anode, cathode or electrolyte. Among of many MOFs, Zn₄O(BTB)₂.(DEF)_m(H₂O)_n (MOF-177) has been studied using for lithium (Li) battery application as an anode. In the decomposition reaction of MOF-177, fairly high irreversible capacity will be produced and along with the formation of by-product of metallic zinc (Pettinari, et al., 2017). Hence, it is a suitable anode material for lithium ion batteries since it possesses with great capacity volume. The reaction is shown as below:



Recently, MOF-based supercapacitors have been developed. Supercapacitor, also known as electrochemical capacitor, is a device used for storing high-power energy with outstanding stability, longer cycle life and higher packing flexibility compared to conventional energy storage devices. MOFs can be destroyed for acquisition of metal-oxides, maintaining the electrons via charge transfer between electrode and electrolyte, like the case of heating up a Co-based MOF (Zhang, et al.,

2011). MOFs can also be pyrolyzed to yield porous carbon that is enhanced in capacity (Jiang, et al., 2011).

2.5 Important Parameters Affecting Structure of MOF

MOFs have arisen as a predominant type of materials that are being utilized in lots of applications because of their fascinating features. However, the synthesis of MOFs with targeted framework structure is still a challenge up until now. In order to appreciate the distinct features and to design new types of MOFs, it is essential to know how to justify the design and synthesis of MOFs from a fundamental perspective.

Thus, it is important to understand what aspects that would like to affect the MOFs structure in order to design desired MOFs frameworks for specific applications. It is well known that the MOFs structure is not only dependent on the modulus building blocks, but they can be affected by many synthesis environments for instance the solvent types, pH environment, reaction temperature, time and pressure of reaction, molar ratio between the metal precursors and organic ligands and etc. Out of these influencing factors, nature of the solvents, pH value, temperature, time and molar ratio of reacting agents are the key factors that control the overall framework structure of MOF.

2.5.1 Effect of Solvents

Solvent type is the utmost important concern in the synthesis of MOFs since they can affect the coordination performance of metal precursors and organic ligands. Numerous research works have been done by the researchers demonstrating that solvent plays an important role in determining the coordination conditions by either directly coordinates with metal precursors or acts as a guest molecule in the formation of lattice structure. But most of the time, the solvent may not take part in the coordination of the MOFs, they just act as a structure formation leading agent in the coordination process of MOFs (Yakovenko, et al., 2014).

Two types of fluorinated MOFs, Cu-F-MOF-4B and F-MOF-4 have been discovered that their formations are dependent on the types of solvents used. In this experiment, two types of solvents, DEF and DMF were used to synthesis these two types of MOFs under the identical reaction conditions. The result confirms that the structures for these two MOFs using different types of solvents are vary and in turn affecting their performance in gas adsorption. This variety in structure formations might be the reason

of the unlike degree of deprotonation of H₂hfbba by using different types of solvents. The extent of deprotonation can be manipulated by choosing the appropriate solvent types or by changing the solvent basicity (Pachfule, et al., 2011).

Furthermore, with the purpose of examining the impact of solvent on coordination structure foundation, an experiment had been conducted on the reaction between biphenyl tricarboxylic acid (organic ligand) and Cd(NO₃)₂·4H₂O (metal precursor) along with three distinct kinds of organic solvents: DMA, DEF and DMF. The outcome is that they are three distinct coordination of MOFs were produced, they are {[Cd₃(BPT)₂(DMF)₂·2H₂O}, [Cd₃(BPT)₂(DMA)₂] and [(CH₃CH₂)₂NH₂]·{[Cd(BPT)]·2H₂O}. Among them, Cd₃(BPT)₂(DMF)₂·2H₂O} is a three-dimensional framework which contains Cd–O–Cd chains with the DMF molecule linking the adjacent Cd₁ and Cd₂ centres; [Cd₃(BPT)₂(DMA)₂] is also a three-dimensional framework, but contains the infinite metal-carboxylate chains with DMA molecule linked to only one of the Cd (II) centres; while [(CH₃CH₂)₂NH₂]·{[Cd(BPT)]·2H₂O} is a two-dimensional framework which analogous to honeycomb net, are stacked together to form a three-dimensional supramolecular structure, as illustrated in Figure 2.7 (Li, et al., 2012 b). Thus, from all these experiment works, we can come to a conclusion that the types of solvent play noteworthy role in regulating the MOFs' coordination structure.

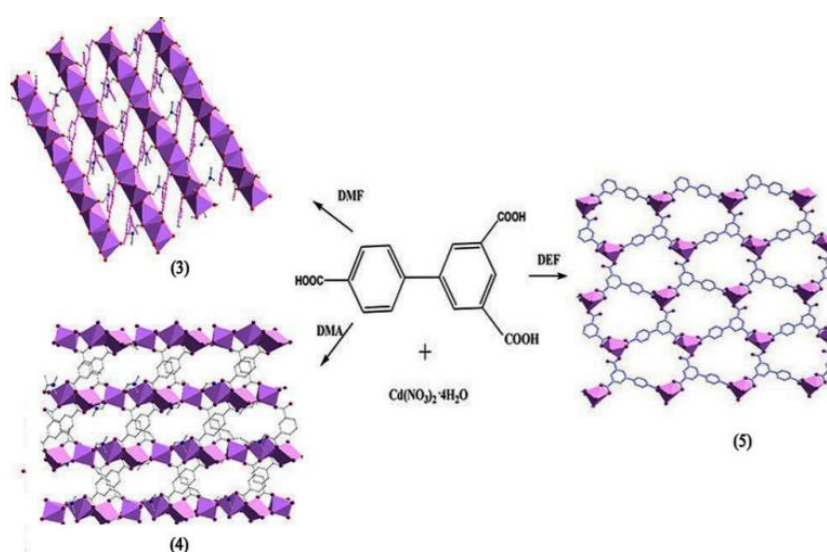


Figure 2.7: (3){[Cd₃(BPT)₂(DMF)₂·2H₂O}, (4) [Cd₃(BPT)₂(DMA)₂] and (5) [(CH₃CH₂)₂NH₂]·{[Cd(BPT)]·2H₂O} formed by using Different Kinds of Solvents: DMF, DMA and DEF correspondingly (Li, et al., 2012 b).

2.5.2 Effect of pH

It is well known that the pH value of reaction mixture would greatly influence the growth of organic and inorganic hybrid materials which subsequently affect the MOFs' crystallization (Li, et al., 2013). Some research works concerning about the effect of pH value to organic ligands' coordination modes have been studied and all these works' outcomes have shown that reaction mixture's pH value has remarkable influence in determining the coordination modes in MOFs' structure.

Three coordination polymers of MOFs with diverse dimensionality and composition were formed under different pH value, they are $[\text{Co}(\text{HADA})_2(\text{bpp})]_n$, $\{[\text{Co}(\text{ADA})(\text{bpp})(\text{CH}_3\text{OH})]\cdot\text{H}_2\text{O}\}_n$ and $[\text{Co}_2(\text{ADA})_2(\text{bpp})]_n$. They were formed under pH values of five, six and seven respectively (Zhang et al., 2010b).

Similar phenomenon was observed in cadmium-based reaction. Two different types of cadmium frameworks were formed by manipulating the reaction pH value: $[\text{Cd}_3(\text{OH})_2(2,4\text{-PYDC})_2]$ was formed under pH value of 8.5 while at the pH of 4.5, $\{[\text{Cd}_2(2,4\text{-PYDC})_2(\text{bde})]\cdot 2\text{H}_2\text{O}\}$ will be formed. This phenomenon is owing to the explanation that the partial and full deprotonation of the ligand will happen at pH value of 1.5 and 2.5 respectively. Nevertheless, when the pH value was increased to between 4 and 5, some hydroxyl group will direct to the Cu (II) ions and the full deprotonation will be induced (Yu et al., 2008).

Other than the coordination modes, the colour of the compound formed is also highly dependent on reaction mixture pH value. Three different colours of Co-BTC-3,3',5,5'-tetra (1H-imidazole-1-yl)-1,1'-biphenyl compounds were produced by manipulating the reaction pH environment: pink coloured crystals of $\{[\text{Co}(\text{L})(\text{HBTC})_2(\mu_2\text{-H}_2\text{O})(\text{H}_2\text{O})_2]\cdot 3\text{H}_2\text{O}\}$ was formed under pH value of five, purple coloured crystals of $\{[\text{Co}_3(\text{L})_2(\text{BTC})_2]\cdot 4\text{H}_2\text{O}\}$ was formed under pH value of seven while brown crystals of $\{[\text{Co}_2(\text{L})(\text{BTC})(\mu_2\text{-OH})(\text{H}_2\text{O})_2]\cdot 2\text{H}_2\text{O}\}$ was formed at pH value of nine (Li, et al., 2013).

2.5.3 Effect of Temperature

Two kinds of Ho (III) succinate coordination polymers, $\{[\text{Ho}_2(\text{C}_4\text{H}_4\text{O}_4)_3 (\text{H}_2\text{O})_4] 6\text{H}_2\text{O}\}$ and $\{[\text{Ho}_2(\text{C}_4\text{H}_4\text{O}_4)_3 (\text{H}_2\text{O})_2] \cdot \text{H}_2\text{O}\}$ had been fabricated under non-hydrothermal and hydrothermal temperature correspondingly. Different dimensionality of the compounds will subsequently affect their magnetic properties and thermal stability. As a result, the thermal stability of $\{[\text{Ho}_2(\text{C}_4\text{H}_4\text{O}_4)_3 (\text{H}_2\text{O})_2] \cdot \text{H}_2\text{O}\}$.

H_2O is higher than $\{[\text{Ho}_2(\text{C}_4\text{H}_4\text{O}_4)_3 (\text{H}_2\text{O})_4] 6\text{H}_2\text{O}\}$, indicating that the hydrothermal condition prone to a more stable framework formation and thus the compound synthesized by using hydrothermal method will have higher thermal stability. Hydrothermal method will form the compound networks with open channel instead of polymeric films that will be likely formed under room temperature condition (Bernini, et al., 2007). Hence, temperature will affect the coordination modes of MOFs.

A research work regarding to the reaction between the Zn (II) ion and 5-iodoisophthalic acid under hydrothermal and room temperature conditions had been carried out. It is concluded that the hydrothermal condition is more towards for obtaining solids with better thermal stability, less hydration, denser and higher dimensionality as compared to the room temperature condition (Zhang, et al., 2012).

Tm-Succinate MOF fabricated by reacting $\text{TmCl}_3 \cdot 6\text{H}_2\text{O}$ with succinic acid under temperature of 100 °C and 180 °C respectively. The used of succinate ligand as organic linker is due to the succinic acid's flexibility and availability of various coordination modes. Although both the temperature conditions produced three-dimensional compounds with same empirical formula, $\{[\text{Tm}_2(\text{L})_3(\text{H}_2\text{O})] \cdot \text{H}_2\text{O}\}$ and also same dimensionality. However, the linking between succinic acid and metal ions is in two discrete manners under different temperature conditions (Figure 2.8) (Carlos, et al., 2013). Hence, controlling the reaction temperature would enable the formation of targeted MOFs with desired dimensionality, coordination structure, thermal stability and other relevant features.

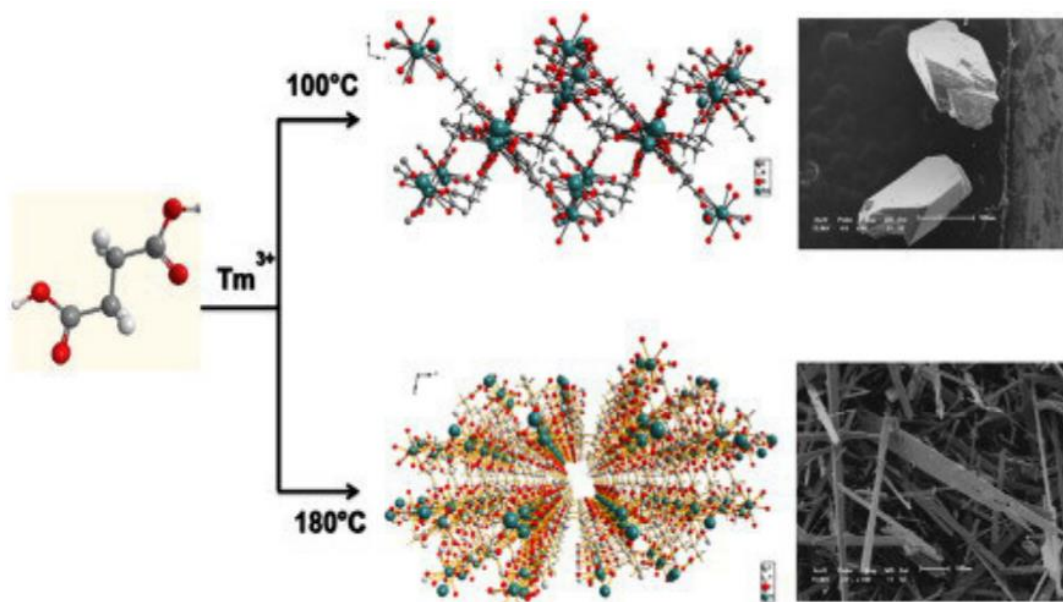


Figure 2.8: Different Tm-succinates Compounds' Coordination Under Different Reaction Temperature, 100 °C and 180 °C (Carlos, et al., 2013).

2.5.4 Effect of Crystallization Time

Crystallization time plays a profound effect on the structural chemistry of ligands and assembly process of ligands with metal centres leading to products with diverse structures. One of the examples is the reaction between $\text{Cd}(\text{NO}_3)_2 \cdot 4\text{H}_2\text{O}$ and 1,3,5-benzenetricarboxylic acid (H_3btc) in DMF at 95 °C at different reaction time would produce different structures of compounds.

When the reaction solution was heated for 10 minutes, a major powder product ($[\text{Cd}(\text{Hbtc})(\text{H}_2\text{O})_2]$) was produced together with a small quantity of crystals deposited ($[\text{Cd}(\text{Hbtc})(\text{DMF})_2]$). When the reaction time was prolonged to one hour, a colourless crystalline material was formed ($[\text{Cd}_3(\text{btc})_2(\text{H}_2\text{O})_9]$). When the reaction mixture was heated for two days, solid with different composition was formed, $[\text{Cd}_{12}(\text{btc})_8(\text{DMF})_{14}(\text{OH}_2)_2] \cdot 1.5\text{DMF}$ (Burrows, et al., 2011).

This experiment result revealed that the dimensionality of the structure increases with increasing reaction time. Heating time of 10 minutes yields two-dimensional networks of $[\text{Cd}(\text{Hbtc})(\text{H}_2\text{O})_2]$ and $[\text{Cd}(\text{Hbtc})(\text{DMF})_2]$, heating for one hour give the bilayer network, $[\text{Cd}_3(\text{btc})_2(\text{H}_2\text{O})_9]$ while heating for two days gives the three-dimensional network of $[\text{Cd}_{12}(\text{btc})_8(\text{DMF})_{14}(\text{OH}_2)_2] \cdot 1.5\text{DMF}$ (Burrows, et al., 2011). Hence, it can be concluded that crystallization time may affect the dimensionality of the MOF samples.

2.5.5 Effect of Molar Ratio of Starting Materials

Molar ratio of the starting materials is a vital aspect affecting the MOFs' topology. Cu-based coordination polymers at controlled molar ratio of ligand to metal had been synthesized, they are $\{[\text{Cu}_4(\text{bpp})_4(\text{maa})_8(\text{H}_2\text{O})_2]_n \cdot 2n\text{H}_2\text{O}\}$, $\{[\text{Cu}_3(\text{maa})_6(\text{bpp})_2]_n\}$ and $\{[\text{Cu}_2(\text{maa})_4(\text{bpp})]_n\}$. $\{[\text{Cu}_4(\text{bpp})_4(\text{maa})_8(\text{H}_2\text{O})_2]_n \cdot 2n\text{H}_2\text{O}\}$ was synthesized with a molar ratio of organic ligand (bbp) to the metal precursors at 2:1, is a neutral, triplestranded molecular braid; $\{[\text{Cu}_3(\text{maa})_6(\text{bpp})_2]_n\}$, which was fabricated with a molar ratio of the of organic ligand to metal precursor at 1.5:1 is an interlaced three-dimensional supramolecular structure consisting of one-dimensional zigzag polymeric; while $\{[\text{Cu}_2(\text{maa})_4(\text{bpp})]_n\}$ compound, which was formed at reactants' molar ratio of 1:1 containing one-dimensional zigzag chains connected with dinuclear nodes (Luan, et al., 2006).

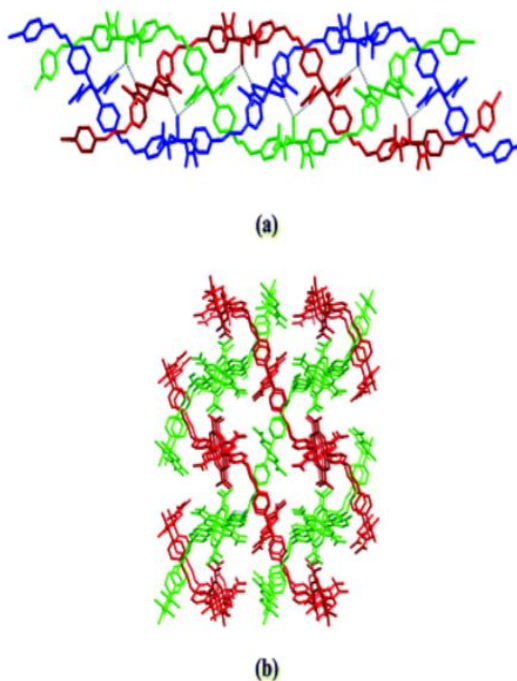


Figure 2.9: Different Cu-Based MOF Coordination Structure Obtained Under Different Molar Ratio of Reactants (Luan, et al., 2006).

In the hydrothermal reactions between Zn metal ions and benzoic acid along with different ratio of co-ligand, 4,4'-dipyridylsulfide, three different kinds of framework structures of Zn-based compounds were produced. Among of these three different framework structures, $[\text{Zn}(\text{hfipbb})(\text{H}_2\text{hfipbb})_{0.5}]_n$ which was synthesized at Zn: H_2hfipbb :dps molar ratio of 1:1:0.25 is a three-dimensional two-fold parallel

interpenetrating pillared network. By adjusting the stoichiometry of co ligand, another two isomeric framework structures $Zn_2(\text{hfipbb})_2(\text{dps}) \cdot \text{H}_2\text{O}]_n$ can be produced which exhibit either non-interpenetrated or interpenetrated bimodal-connected network (Figure 2.10) (Wu et al., 2011).

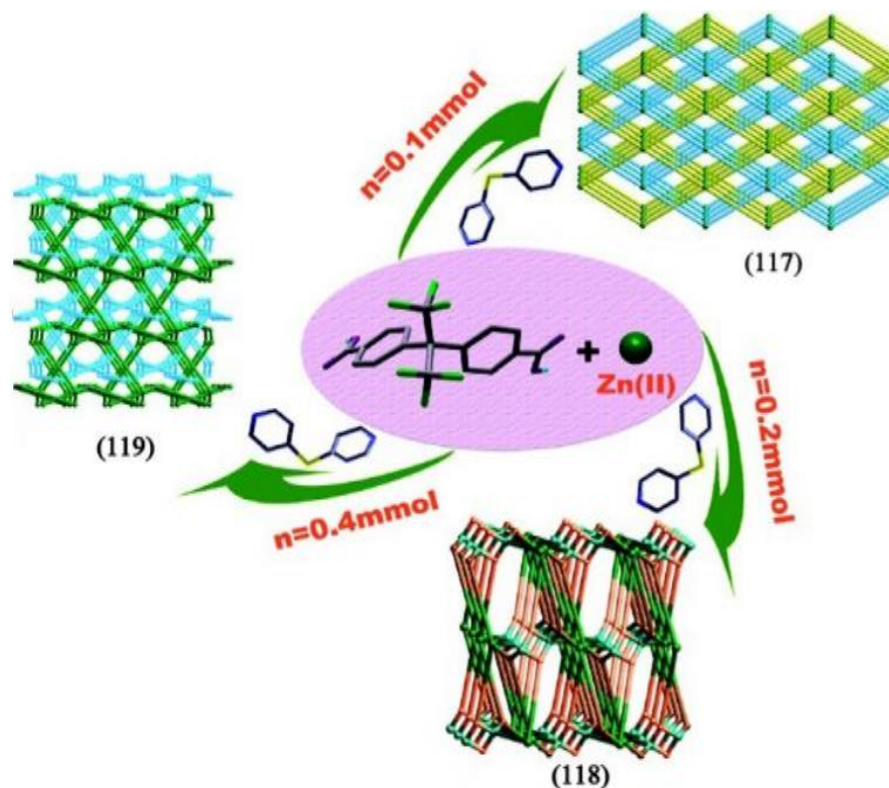


Figure 2.10: Different Zn-Based MOF Coordination Structure Obtained by Varying the Stoichiometry of Co-ligand (Wu, et al., 2011).

2.6 MOF Synthesis Methods

So far, MOFs are usually prepared by utilizing hydrothermal/solvothermal method, it is the most common method used in synthesizing MOFs in laboratory. However, due to its drawbacks including long reaction time from several hours to days, low quality of products obtained, requirement of large amount of solvents, difficulty in scaling-up. All these factors have motivated many researchers to develop alternative synthesis methods to shorten the crystallization time, to yield smaller and more uniform crystal products. Figure 2.11 shows the most common synthetic methods utilized currently.

It is well known that each method will result in different morphology, particle sizes and size distributions of MOFs and in turn lead to diverse applications. Hence,

each method's reaction conditions as well as their advantages and disadvantages need to be prior studied before synthesizing targeted MOFs with desired framework structures.

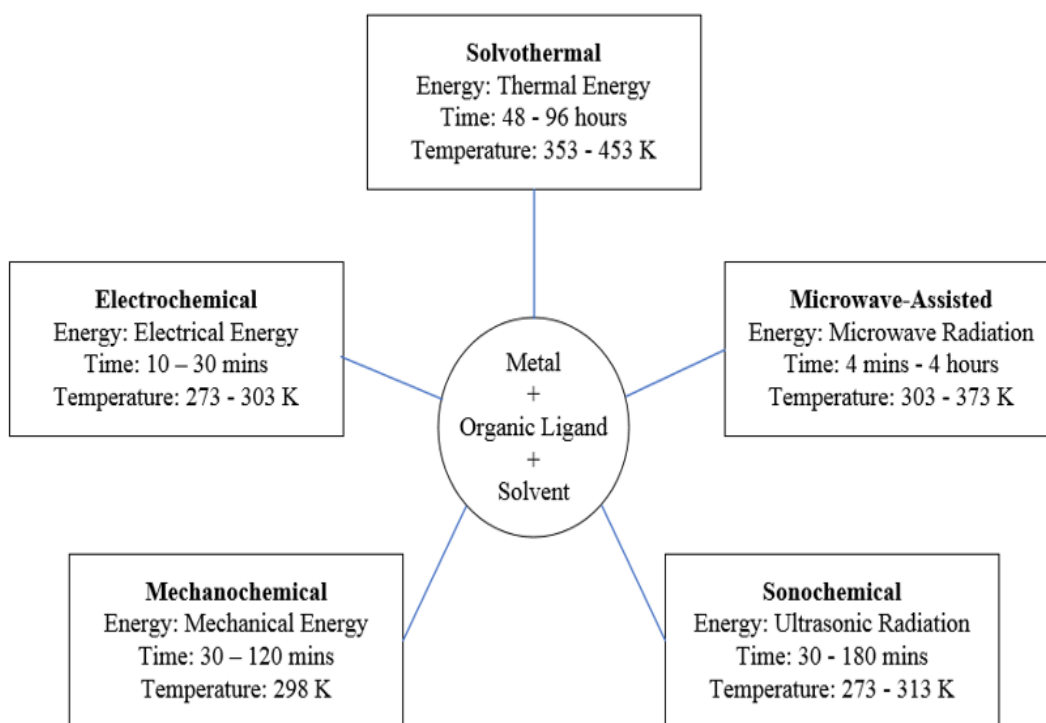


Figure 2.11: MOF Synthesis Methods and Their Respective Synthesis Conditions.

2.6.1 Hydrothermal/Solvothermal Method

Hydrothermal also known as solvothermal method, it requires reaction condition of high pressure and high temperature of greater than 100°C. Normally, the reaction takes place in vials, sealed NMR tubes or closed vessel, known as Teflon lined autoclave and kept for a duration of several hours or days. Since the reaction is happened under high temperature, high boiling point solvents, such as Diethyl formamide (DEF), Dimethyl Sulfox (DMSO), Dimethylformamide (DMF), H₂O, acetone and alcohol are used. If the reacting materials' solubilities are different, then a mixture of these solvents will be used.

This method offers advantages including of high precursors solubility and able to form good quality of MOF crystallite particles, which are easy for structural characterization purpose. Although hydrothermal method is extensively used in lab-scale experiments due to its advantages stated above, it is not preferred in large-scale

production of MOFs due to low product yield, energy intensive and lengthy reaction time (Bo, et al., 2015).

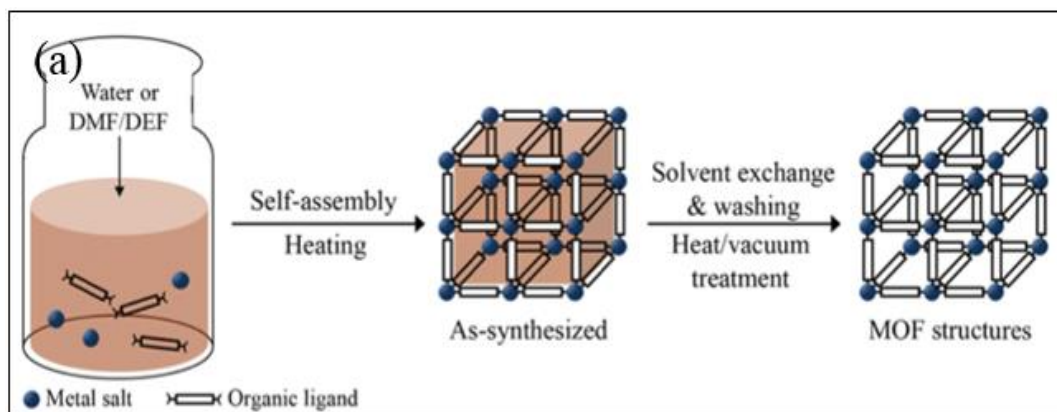


Figure 2.12: Schematic Diagram of Solvothermal Method (Lee, Kim and Ahn, 2013).

2.6.2 Microwave-assisted Method

This method employs high frequency of electromagnetic waves ranging from 300 MHz to 300 GHz for a period of about an hour to synthesize MOFs. Different from the conventional hydrothermal method, where the thermal energy is transferred from the heat source to the reactants through the reaction vessel, in microwave-assisted synthesis, the irradiation energy directly interacts with the reactants, hence it is more energy efficient and rapid synthesis route for MOF. This methodology has been widely employed in obtaining the nano-sized MOFs with identical morphology, high purity and very uniform size distribution (Klinowski, et al., 2011).

In microwave-assisted synthesis, a substrate mixture along with solvent is transferred to a closed vessel and placed in the microwave unit, then heated for certain time at the set temperature. When the microwave is applied, dipole moment of the precursors inside a vessel tube will rotate by itself to align with this microwave field. Frequent alignment collisions between the precursor molecules will lead to accumulation of kinetic energy and thus increasing the sample temperature. This is the overall scheme for the energy translation from electromagnetic energy to thermal energy. Advantages for this method is adjustable in power outputs, reaction pressure and temperature (Liang and D'Alessandro, 2013).

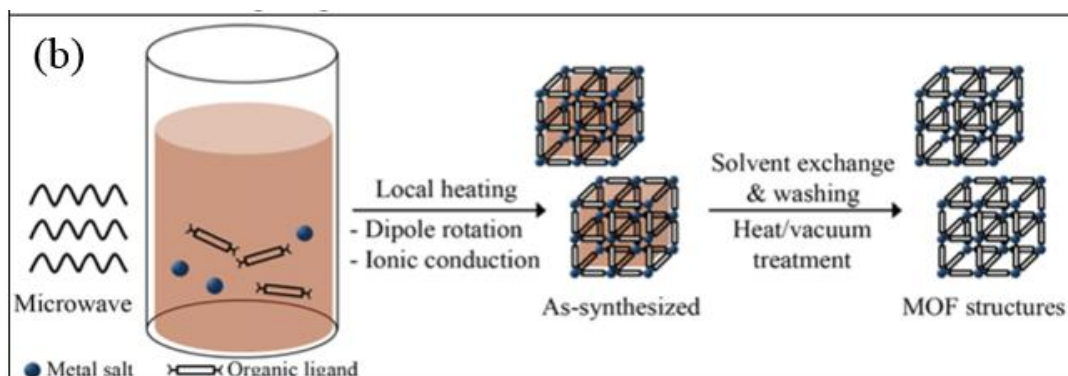


Figure 2.13: Schematic Diagram of Microwave-assisted Method (Lee, Kim and Ahn, 2013).

2.6.3 Sonochemical Method

Sonochemical method also known as ultrasonic method, is a technique employing strong ultrasonic radiation in the frequency between 20 kHz and 10 MHz to induce chemical or physical changes of molecules. This process of chemical or physical change in the liquid molecules is called as cavitation. Under this process, bubbles will grow and collapse throughout the liquid medium when sonication is applying. The collapse of these bubbles will rapidly release energy with temperature of around 400 K and pressure up to 1,000 atm (Bigdeli and Morsali, 2015).

A substrate reaction mixture is transferred into a hom-type Pyrex reactor fitted to a sonicator bar (Figure 2.14). When the sonication is applied, acoustic bubbles will form and collapse in the liquid mixture, and produce very high local temperature and pressure at the same time. Thus, this whole process will result in tremendously fast heating and cooling rates, end up producing very fine MOF product.

Sonochemical is an energy efficient and environmental-friendly way of MOF fabrication. Besides, it is also a rapid way of synthesizing MOFs since the application of ultrasound has shortened the crystallization time (Karizi, Safarifard and Morsali, 2015).

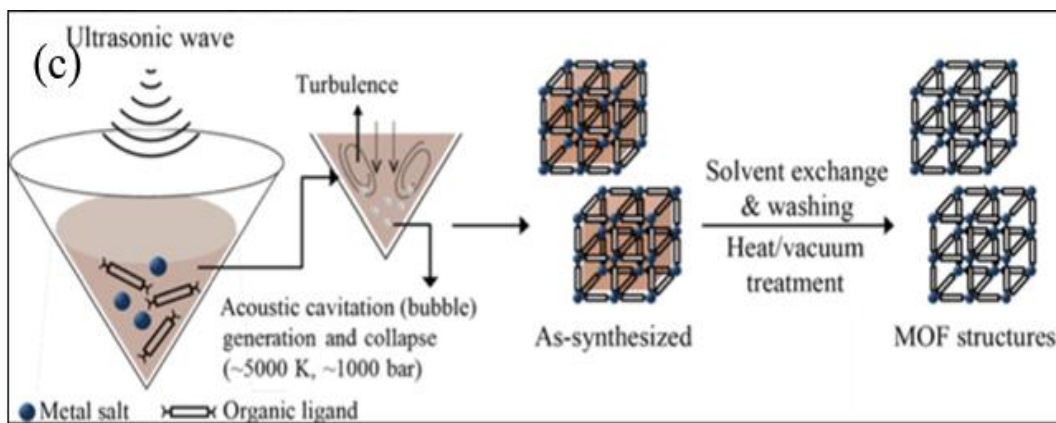


Figure 2.14: Schematic Diagram of Sonochemical Method (Lee, Kim and Ahn, 2013).

2.6.4 Electrochemical Method

Electrochemical method utilizes two electrodes, anode and cathode, as well as an electrolyte in the fabrication of MOFs. Metal ions instead of metal salts are continuously provided through anodic dissolution when voltage is supplied to the electrodes, react with the dissolved organic linker molecules under this electrochemical synthesis. These metal ions will react with electrolyte and organic ligands to form micro crystalline MOF powders and films (Joaristi, et al., 2012).

The major advantage for this method is the continuous formation of MOFs, which enables the mass production of MOF materials. Besides, this electrochemical reaction can be happened under lower pressure and temperature, thus reducing energy consumption (Carson, et al., 2011)..

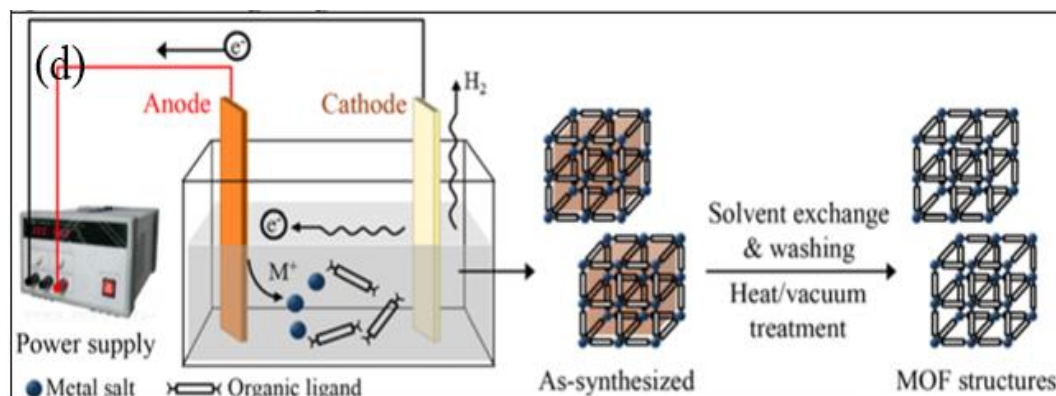


Figure 2.15: Schematic Diagram of Electrochemical Method (Lee, Kim and Ahn, 2013).

2.6.5 Mechanochemical Method

Mechanochemical is a solvent-free MOF synthesis way in which the mechanical force is adopted to grind and mill the mixture of metal precursors and organic ligands together to promote the chemical reactions. Under this mechanical grinding process, the intramolecular bonds of starting materials will be broken, and new bonds will form. With this method the conventional solvothermal reactor will be replaced by a mortar and pestle or ball mill (Klimakow, et al., 2010).

They are three different approaches under this mechanochemical synthesis. Solvent-free Grinding (SFG), which is the simplest solvent free method. The most noteworthy advantage for this method is to produce MOF with water as the only by-product if metal oxide or hydroxides is used rather than the metal salt. The oxides or hydroxides of metal will react with the proton in organic ligands to form water. For Liquid-Assisted Grinding (LAG), liquid will be added in to accelerate the mechanochemical reaction by improving the mobility of precursors. In addition, the liquid also acts as structure-directing agent. Hence, it is a quicker and more versatile approach. The last one would be Ion-and-Liquid Assisted Grinding (ILAG) in which uses liquid together with traces of salt additives to accelerate the formation of MOF.

Mechanochemical approach is the simplest, most economical and environmental-friendly way of MOFs fabrication as compared to liquid phase synthesis methods. In addition to the solvent-free condition, this method enables the use of low-solubility MOF precursors and quantitative yields of products. Besides that, this method can be taken place under room temperature within short period of synthesis time and its side products are harmless (Pilloni, et al., 2015). However, this method is limited to specific types of MOF only and its production is difficult to be scaled-up.

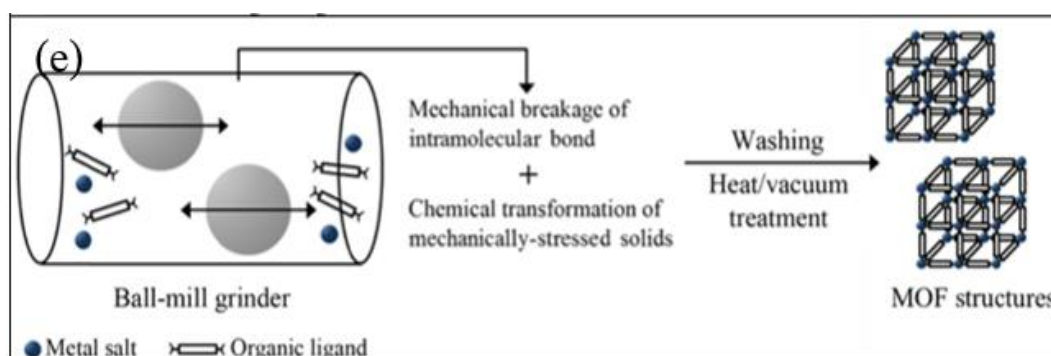


Figure 2.16: Schematic Diagram of Mechanochemical Method (Lee, Kim and Ahn, 2013).

2.7 Properties of MOFs in Carbon Dioxide Gas Adsorption

Under this section, some vital MOFs' structural properties relating to the carbon capture application are highlighted. These aspects are important parameters that need to be taken into account when assessing new materials for carbon dioxide gas capture application.

2.7.1 Capacity for CO₂

Capacity for CO₂ gas adsorption is the utmost important parameter when assessing a type of MOF as a suitable adsorbent for CO₂ gas capture. Due to the dense packing and strong attachment of the guest molecules on the metal-organic frameworks' pores surface, it can have high internal surfaces. These high internal surfaces have provided them with great CO₂ gas adsorption capacity (Kenji.S, 2011). For instance, MOF-177, which have high volumetric CO₂ adsorption capacity of 320 cm³/cm³. Its capacity is about nine folds larger than that of the conventional materials that are employed for this gas adsorption application, such as zeolites (Millward and Yaghi, 2005).

2.7.2 Selectivity for CO₂

Apart from the high gas adsorptive capacity, high selectivity towards CO₂ gas over the other gas components, such as H₂ and CH₄ is essential in CO₂ gas capture application. This selectivity is made up of two mechanisms, namely adsorptive selectivity and size-based selectivity.

Adsorptive selectivity, also known as thermodynamic separation, it works by relying on difference in gas component physical properties, for example the

polarizability and quadrupole moment. This difference in physical properties would result in discrete levels of affinity of gas components towards the pores surface of MOFs. For example, in the separation of CO₂ gas and N₂ gas mixture, CO₂ possesses higher quadrupole moment and polarization than N₂. Hence, the surface of material shows higher affinity towards the CO₂ gas molecules and adsorbs the gas molecules on its surface.

While in size-based selectivity (kinetic separation), it works by relying on the size difference of molecules. This type of selectivity only allow the diffusion of the molecules that are small enough in kinetic diameter into the pores while the larger molecules cannot enter the pores and hence could be separated out (Kenji.S, 2011).

Besides, their chemical interaction with the metal-organic frameworks surface functionalities also play a significant role in adsorptive selectivity (Kenji.S, 2011). MOF surface functionalities can identify certain gas components molecules, which exhibit higher tendency in participating the reaction and thus result in a higher selectivity over the other gas components.

2.7.3 Coordinatively Unsaturated Metal Sites

MOFs with coordinatively unsaturated metal sites make use of Lewis acidity. Lewis acidity can provide metal sites with partial positive charges and therefore can display comparatively high CO₂ adsorption heats at lower pressure. In other words, coordinatively unsaturated metal sites of MOFs can provide with high CO₂ gas capacity and selectivity since it can form a stronger electrostatic interaction with CO₂ gas molecules (Trickett, et al., 2017).

Mg-MOF-74 is one of the well-studied MOFs in this aspect. It can adsorb the greatest amount of CO₂ gas under the standard temperature and pressure ever reported. Its high CO₂ gas adsorption capacity is due to the availability of the coordinatively unsaturated metal sites which permit the efficient binding of CO₂ gas molecules onto them (Caskey, Wong-Foy and Matzger, 2008). Its structure is illustrated in the Figure 2.17.

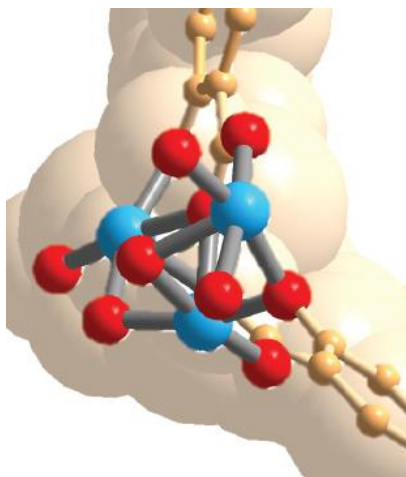


Figure 2.17: Structure of Mg MOF 74 with Unsaturated Metal Sites Coordination (Trickett, et al., 2017).

2.7.4 Enthalpy of Adsorption

The adsorption enthalpy is another important consideration when assessing the CO₂ gas capture performance of an adsorbent material. Its magnitude is an indication of the affinity of the pore surface of the given material towards CO₂ gas, which in turn affects the adsorptive selectivity and the amount of energy required to release the CO₂ gas molecules during the regeneration process.

Binding strength of CO₂ gas to pore surfaces of the given material must be accurately controlled. If the magnitude of adsorption enthalpy is too high, a material will bind too strongly with CO₂, which in turn increasing the regeneration cost since large amount of energy is required to break the connection; however in the opposite way, if the magnitude of adsorption enthalpy is too low, other gas components other than carbon dioxide gas will be adsorbed on the adsorbent surface and thus causing decrease in the selectivity. Hence in response, a greater volume of adsorbent material would need to adsorb the required quantity of CO₂ (Kenji.S, 2011).

2.8 Characterization Techniques and Instrumentations

Basically, characterization techniques are made up of two broad classes: physical characterization and chemical characterization techniques (Figure 2.18). SEM and XRD belong to physical characterization category in which can determine the sample physical properties; EDX and FTIR are chemical characterization instrumentations that can be used to examine the chemical properties of samples while TGA can provide both physical and chemical information of the sample.

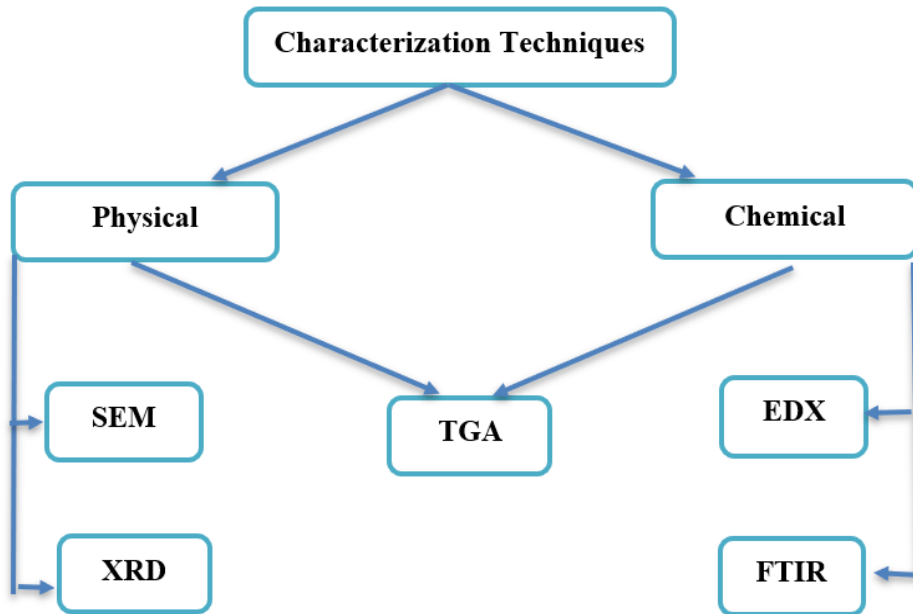


Figure 2.18: Categories of Characterization Techniques.

2.8.1 Scanning Electron Microscope Coupled with Energy-Dispersive X-ray Spectrometer (SEM-EDX)

SEM is a scientific apparatus that uses highly energetic electron beam to examine the surfaces of materials on a very fine scale. It can be utilized to reveal the information about the samples including composition, crystallographic, topography and morphology.

Topography is the surface structures of an object while morphology is the size, shape and arrangement of the particles that are lying on the sample surface. Both topography and morphology detectable features limited to a few nanometres by using SEM. The components that are making up the sample and their relative ratios can be determined with the help of EDX in areas of about a micrometre in diameter. Alternatively, the crystallographic of a sample can be determined by using SEM, but this can only be applied on single-crystal particles that are greater than 20 micrometres.

SEM works by forming an electron beam and accelerating it towards the sample. This electron beam is then confined and focused using magnetic lenses into a focused, monochromatic beam. Inside the specimen, interactions will occur upon irradiated by the electron beam. Thus affecting the scattering direction and strength of electron beam and produce different kinds of signals, including of backscattered electrons, Auger electrons, secondary electrons and X-rays, which carry different

kinds of information of the sample (Susan, 2017). Figure 2.19 shows the phenomenon happens when the incident electron beam reaches and interacts with the sample specimen surface.

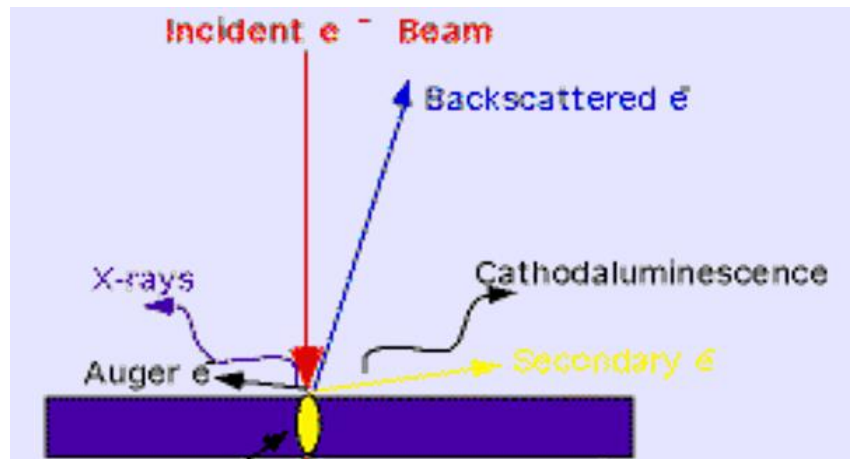


Figure 2.19: Specimen Interaction in SEM.

2.8.2 X-ray Diffractometer (XRD)

X-ray powder diffraction (XRD) is principally adopted for identifying the unknown components inside the sample by comparing the diffraction peaks of a sample against the database maintained by the International Centre for Diffraction Data. Furthermore, it can be applied to characterize crystallite size, determine the phase of a crystalline material and relative abundance of crystalline compounds. The analysed sample material must be finely grounded and in homogenous. (Dutrow and Clark, 2019).

Bragg's Law is commonly adopted in XRD technique for describing the constructive interference of the ordered lattice. It can enable the calculation of the lattice spacing, in which providing information for further phase identification purpose by illustrating the diffraction of X-rays by lattice planes. Diffraction of X-rays happens when the radiated X-rays reach at the atoms underlying on the surface of the sample lattice, the atoms will constructively interfere with the X-rays and hence causing it to be reflected in all directions. Hence, the sample will rotate during the XRD measurement to maximize the amounts of atoms that contribute to the diffraction.

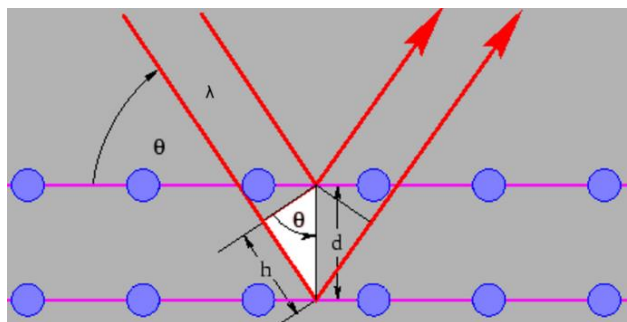


Figure 2.20: Bragg's Law Diagram.

There are some limitations for the application of XRD in sample characterization. It cannot detect either too small or amorphous particles. Besides that, for the sample which owns insufficient long-range order, its diffraction peaks would be unclear and thus unable to be identified. Furthermore, since the XRD technique unable to detect the element existing in the sample that is less than 5 % in composition, some minor phases that exist in the sample may be undetected. (Dutrow and Clark, 2019).

2.8.3 Fourier-Transform Infrared Spectrometer (FTIR)

Infrared light is applied by FTIR technique for imaging the specimen to determine the chemical features of the specimen. The working principle for FTIR technique is to direct a beam of infrared radiation with frequency of about $10,000$ to 100 cm^{-1} through the targeted specimen. The sample will capture almost all this radiation energy while the remaining will pass through the sample. The specimen molecules will transform the absorbed radiation energy into vibrational energy and rotational energy. These transition between vibrational levels will be detected and displays as a spectrum. Each spectrum represents a molecular fingerprint of a sample and the energy frequency shown in the spectrum typically is from $4,000\text{ cm}^{-1}$ to 400 cm^{-1} . Hence, the result for the FTIR analysis would be in the form of spectral fingerprint, which is unique to the specimen molecules (RTI Laboratories, 2015).

FTIR technique is mainly on recognizing the adsorbed species on the sample and studying how these species are chemisorbed on the surface of samples. Besides that, FTIR is a well-known instrumentation applied in goods manufacturing industry. It can be used to examine the quality of the produced goods since the composition change and presence of contamination within the items will exhibit a clear change in the characterized adsorption bands (RTI Laboratories, 2015).

2.8.4 Thermal Gravimetric Analyzer (TGA)

Thermogravimetric analyser measures the weight changes of sample over time as the temperature changes. The changes in sample weight may be caused by the changes in either chemical or physical properties. Hence, by measuring the changes of weight of the sample over time, some information of the sample, such as chemisorption, thermal stability, phase change and etc can be revealed (Scientific, Eurofins, 2018).

TGA is a useful tool in the investigation of material thermal stability under conditions of ramping temperature. Mass, temperature and time are considered as base measuring parameters in TGA while additional measurements may be resulting from these three base measurements. Besides the ramping temperature condition, TGA can also be conducted at constant temperature over a specific period of time to examine materials' thermal stability. The thermal stability test may take place under a variety of atmospheres and pressures (Scientific, Eurofins, 2018).

2.9 MIL-101 (Cr) MOF

MIL-100 and MIL-101 belong to chromium terephthalate metal-organic framework, MIL is the abbreviation for Material Institute Lavoisier. MIL-100 was first discovered by Ferey in 2004 by using hydrothermal method. The structural framework of MIL-100 is illustrated in Figure 2.21, it consists of trimeric chromium (III) linked with benzene-1,3,5-tricarboxylic acid (BTC) molecules. It has unique hierarchical pore system and large surface area (Bhattacharjee, et al., 2014).

Soon after, MIL-101 was later prepared by Ferey and his co-workers in 2005. Its framework structure is quite similar to MIL-100, consists of an augmented MTN zeotype architecture with trimeric chromium (III) octahedral interconnected by BDC molecules (Figure 2.21). Within this structure, two types of mesopores with diameters of 2.9 and 3.4 nm could be accessed through two different kinds of micropore windows (pentagonal window and hexagonal window) of 1.2 and 1.6 nm (Figure 2.22) (Bhattacharjee, et al., 2014).

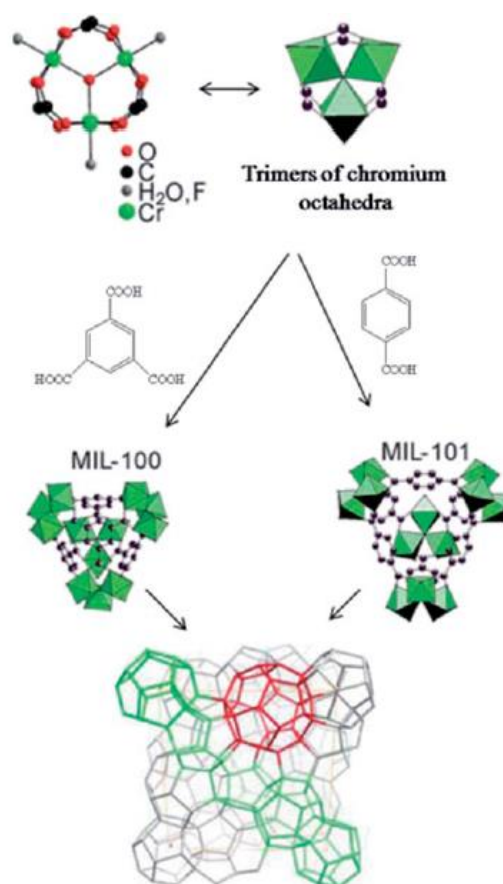


Figure 2.21: MIL-100 and MIL-101 Structural Frameworks (Bhattacharjee, et al., 2014).

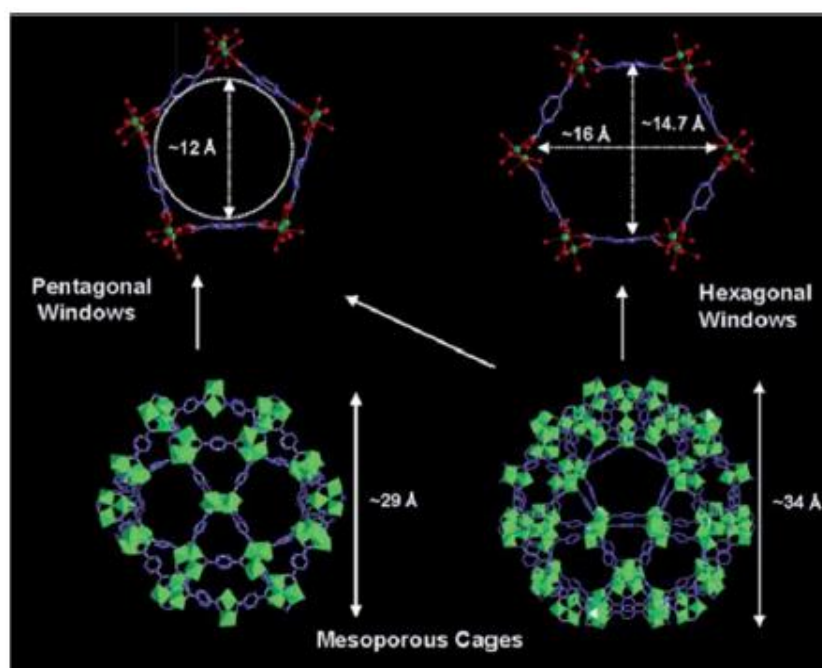


Figure 2.22: Illustrations of Pentagonal Window and Hexagonal Window (Bhattacharjee, et al., 2014).

MIL-101 exhibits large pores size, high Langmuir surface area of greater than $3000\text{m}^2/\text{g}$, huge pore volume, numerous coordinatively unsaturated metal sites, high thermal and chemical stability (Bhattacharjee, et al., 2014). These advantages have made MIL-101 an attractive candidate material for the application of gas adsorption/separation, heterogeneous catalysis and energy storage.

The first reported MIL-101 (Cr) fabricated by Ferey was carried out with the addition of hydrofluoric acid (HF) under hydrothermal condition at $220\text{ }^\circ\text{C}$ for duration of 8 hours. Later, Bromberg discovered a new way of synthesizing MIL-101 (Cr) without the addition of HF. However, this new synthetic way requires four times greater amount of water as that required in the presence of HF and a longer crystallization time of up to 20 hours. In the most currently work reported by Xu and co-workers, MIL-101 (Cr) can be rapidly fabricated without the addition of solvent and HF at 220°C in 4 hours (Leng, et al., 2016).

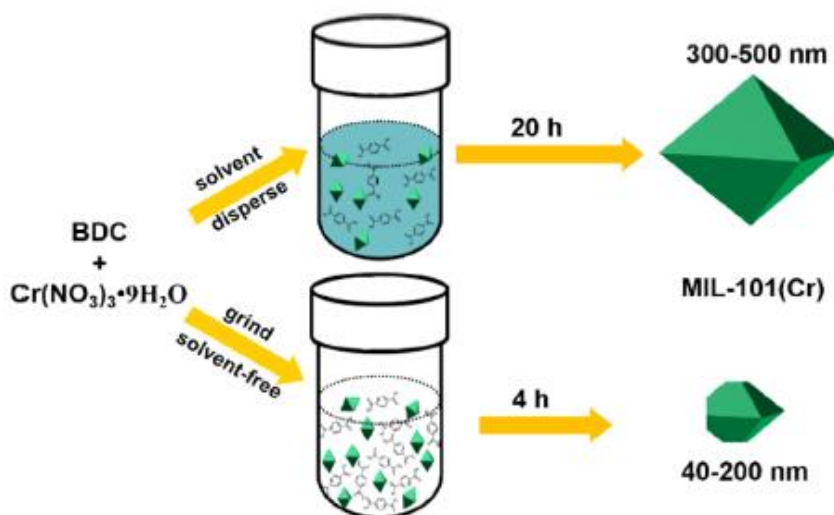


Figure 2.23: Schematic Diagram of Hydrothermal and Mechanochemical Synthetic Process of MIL-101 (Cr) MOF (Leng, et al., 2016).

2.10 UiO-66 (Ce) MOF

In 2008, University of Oslo discovered UiO-66, which is the first zirconium-based MOF (Zr-MOF), it is formed with zirconium (Zr) as metallic nodes while terephthalic acid as the organic linker. Its pore network system consists of large octahedral pores and smaller tetrahedral pores connected by triangular windows (Islamoglu, et al., 2017).

The UiO-66 MOF exhibits high chemical, thermal and mechanical stability as compared to other known MOFs. Furthermore, its tunable porosity and variety functionalities have motivated many researchers to discover and develop wide variety structures of Zr-MOFs based on different clusters. At the same time, Ce (IV) based MOF started to develop rapidly as well since the isostructure of Ce based MOF homologous to the Zr-MOFs and it possesses with exceptional good stability. In addition, cerium (Ce) is the most abundant and low-cost rare-earth metal element (Lammert, et al., 2015).

In 2015, Stock and his co-workers reported the DMF synthesis of UiO-66 MOFs with Ce instead of Zr as metallic node, UiO-66 (Ce) (Lammert, et al., 2015). Figure 2.24 illustrates the DMF synthetic process of UiO-66 (Ce) MOF.

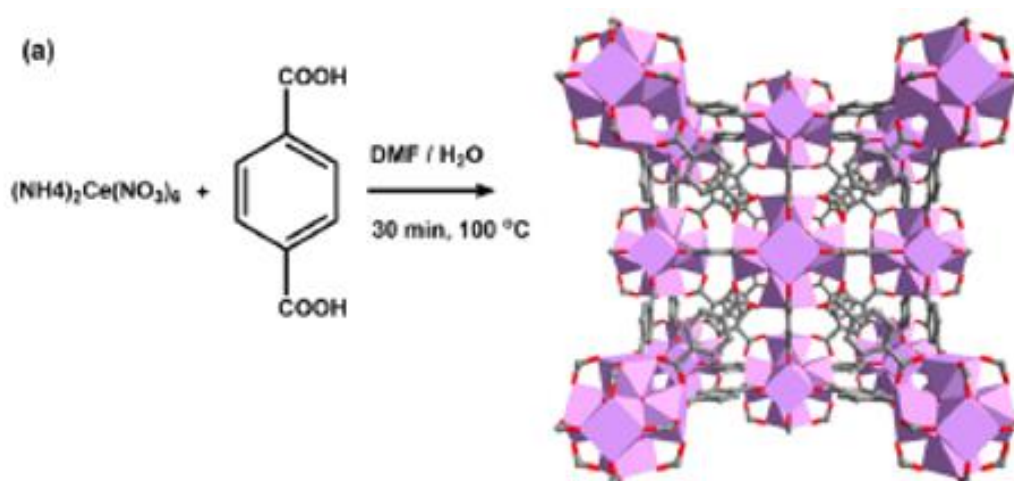


Figure 2.24: Structural Framework of Ce-UiO-66 (Islamoglu, et al., 2017).

In the recent work, a solvent-free method for the synthesis of Ce based UiO-66 MOF was reported. The MOFs are able to be obtained by simply grinding the cerium ammonium nitrate (CAN) and the carboxylic linkers in a mortar and pestle for few minutes with the addition of small amount of acetic acid as modulator. Then the mixture is introduced into a vial and heated at 120 °C for 24 hours (Campanelli, et al., 2019). This is a new green, solvent-free synthetic methodology for crystalline Ce based UiO-66 MOF.

CHAPTER 3

METHODOLOGY AND WORK PLAN

3.1 Materials and Chemicals Used for MOFs Synthesis

3.1.1 Materials and Chemicals for the Preparation of MIL-101(Cr)

Chromium (III) Nitrate Nonahydrate, $\text{Cr}(\text{NO}_3)_3 \cdot 9\text{H}_2\text{O}$ (99 %) and 1,4-Benzene Dicarboxylate (BDC) (98 %), which acted as metal precursor and organic linker respectively were purchased from Sigma-Aldrich. The washing solvent, Ethanol (EtOH) with purity of 95 % was purchased from VWR International.

3.1.2 Materials and Chemicals for the Preparation of UiO-66(Ce)

Both Cerium Ammonium Nitrate (CAN) (98.5 %) and 1,4-Benzene Dicarboxylate (BDC) (98 %) were purchased from Sigma-Aldrich. The washing solvents, Dimethylformamide (DMF) (99.8 %) and Acetone were purchased from Supelco and QRec respectively.

3.2 Preparation of Metal-Organic Frameworks

3.2.1 Preparation of MIL-101(Cr) MOF

Preparation of MOF MIL-101(Cr) is carried according to the procedures reported by Leng et al. (2016). Firstly, $\text{Cr}(\text{NO}_3)_3 \cdot 9\text{H}_2\text{O}$ and BDC were mixed together and grounded under room temperature for approximately 30 minutes. Then, the mixture was introduced into an autoclave and heated at 220 °C for crystallization to be happened. Further, the obtained solid crystals were cooled to room temperature. After it had been cooled down to room temperature, wash it with hot ethanol at 60 °C for 6 hours for eliminating any unreacted reactants. Lastly, the obtained green powders were dried at 120°C for 12 hours.

Based on the difference in the Cr/BDC molar ratio and the crystallization time, each sample will be labelled as MIL-101-A-B. A represents the molar ratio of Cr/BDC while B represents the crystallization time in hour unit. Figure 3.1 illustrated the overall steps for the preparation of MIL-101(Cr)

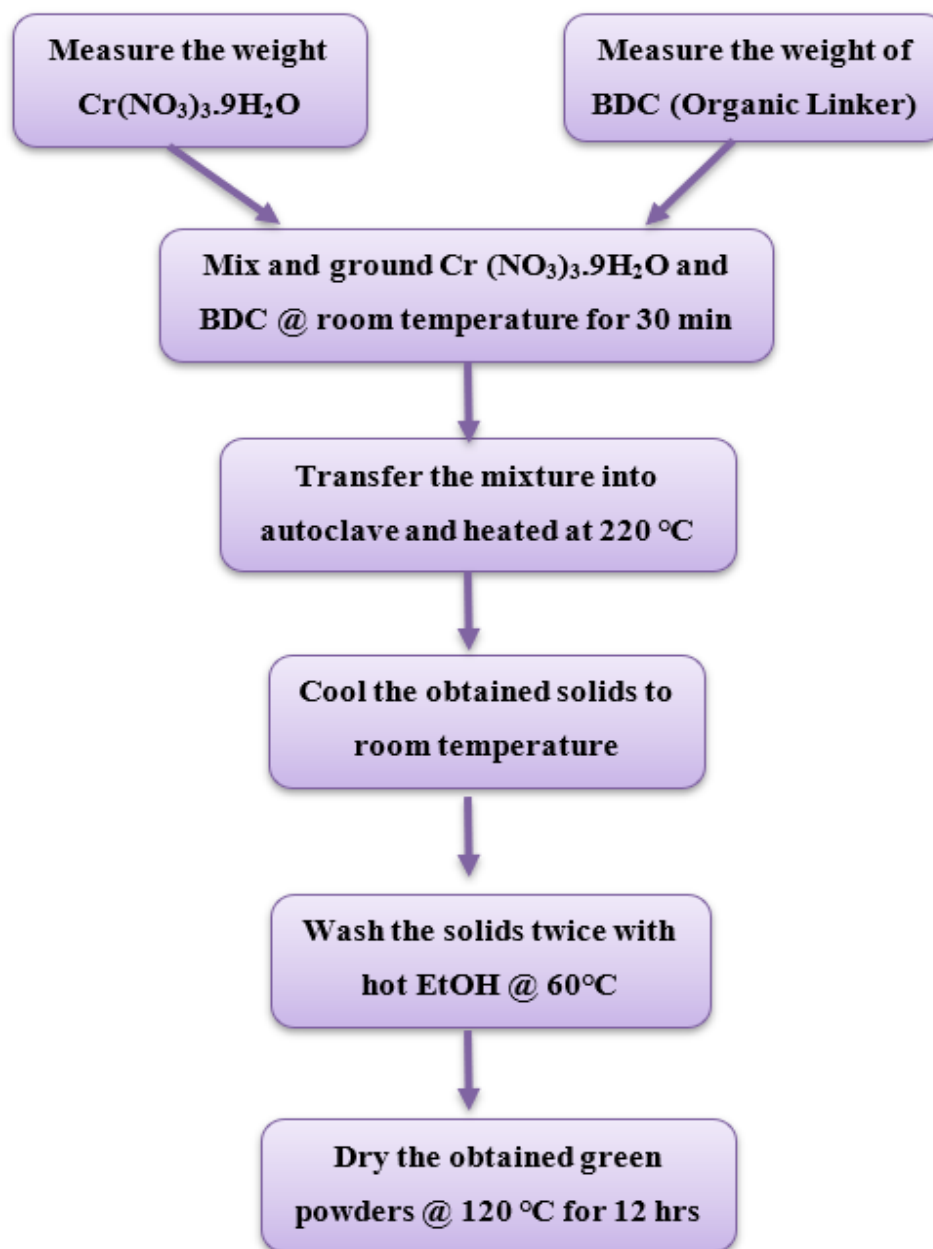


Figure 3.1: Flowchart for the Preparation of MIL-101(Cr) MOF.

3.2.2 Preparation of UiO-66(Ce) MOF

Ce-UiO-66 MOF can be obtained by grinding the cerium ammonium nitrate (CAN) and BDC in a mortar for few minutes. A small amount of acetic acid, which acts as modulator was added as well during the grinding process. Then the slurry mixture was transferred to a Teflon cup and heated at 120 °C for one day. After heating for one day, the orange yellow solids were washed with DMF and Acetone respectively for one time in a centrifuge ($\times 15$ min, 5500 rpm) to recover off-white slurry, Afterwards, the off-white slurry was placed in an oven for drying at 60 °C for 3 hours.

Based on the difference in the CAN/BDC molar ratio and the amount of acetic acid added (0 or 30 wt% equivalent to BDC), each sample will be labelled as Ce-UiO-66-A-B. A represents the molar ratio of CAN/BDC while B represents the weight percentage of acetic acid with respect to BDC. The overall preparation steps for this kind of MOF is illustrated in Figure 3.2 below.

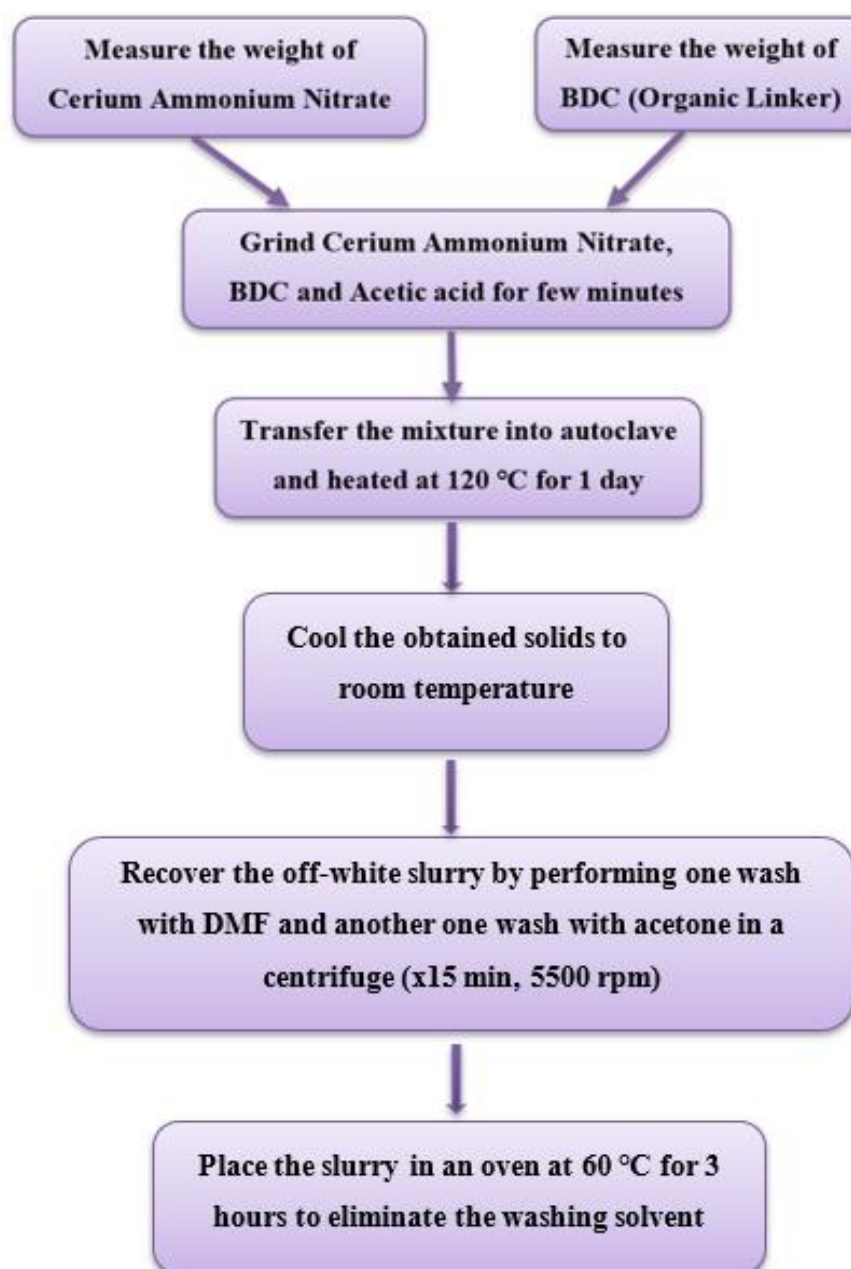


Figure 3.2: Flowchart for the Preparation of Ce-UiO-66 MOF.

3.3 Parameters Study

3.3.1 Parameters Study of MIL-101(Cr) MOF

The study of MIL-101 (Cr) MOF will be divided into two parts. The first part would be the study on the effect of Cr/BDC molar ratio towards the CO₂ gas adsorption performance. While the second part is to investigate on the synthetic parameter of crystallization time.

With the intention of studying the effect of molar ratio between the metal precursors and organic ligand, seven different Cr/BDC molar ratio of MIL-101(Cr) MOFs will be fabricated and tested on their carbon dioxide gas adsorption properties, they are 0.2:1, 0.25:1, 0.5:1, 1:1, 1.5:1, 2.:1 and 2.5:1. These seven different molar ratio of MOFs will be prepared based on same preparation route as shown in Figure 3.1 and the crystallization time is fixed at 4 hours. Hence, these seven samples will be labelled as MIL-101(Cr)-0.2-4, MIL-101(Cr)-0.25-4, MIL-101(Cr)-0.5-4, MIL-101(Cr)-1-4, MIL-101(Cr)-1.5-4, MIL-101(Cr)-2-4 and MIL-101(Cr)-2.5-4 respectively.

In order to find out the most appropriate crystallization time for the formation of MIL-101 (Cr) MOF, the samples fabricated previously with the most outstanding gas carbon dioxide adsorption performance would be further studied on the crystallization time synthetic parameter. On this study, four samples with the crystallization time of 2 hours, 4 hours, 6 hours and 8 hours will be prepared and labelled as MIL-101(Cr)-1-2, MIL-101(Cr)-1-4, MIL-101(Cr)-1-6 and MIL-101(Cr)-1-8 correspondingly.

3.3.2 Parameters Study of UiO-66(Ce) MOF

The molar ratio between cerium ammonium nitrate (CAN) and 1,4-benzenedicarboxylic acid (BDC) is manipulated in order to investigate the effect of reacting agents' molar ratio on the CO₂ gas adsorption capacity in the study of UiO-66 (Ce) MOF. Apart from that, the effect of adding the modulator, acetic acid during the MOF synthesis towards the gas adsorption property is investigated as well in the study of Ce-UiO-66 MOF. A series of samples are synthesized by adding acetic acid as modulator (30 wt% with respect to the amount of BDC added) while another set of samples without the addition of acetic acid to compare the gas adsorption property between the samples with and without addition of acetic acid as modulator.

3.4 Characterization Techniques and Instrumentations

Several characterization techniques and instrumentations were applied throughout this study to examine the physical and chemical features of the MOFs, including of X-Ray Diffractometer (XRD), Scanning Electron Microscope (SEM), Energy-Dispersive X-ray Spectrometer (EDX), and Fourier-Transform Infrared Spectrometer (FTIR).

3.4.1 Scanning Electron Microscope Coupled with Energy-Dispersive X-ray Spectrometer (SEM-EDX)

Hitachi S-3400N Scanning Electron Microscope coupled with EDX was employed in this work to study the composition, morphology and topography of the MOF samples. Prior to the test, small amount of the sample powders was placed on the sample holder by using carbon tape. Then this sample holder was placed in the sputter coater to coat a thin layer of gold and platinum on top of it to improve the sample conductivity. After that, the sample holder was placed into the SEM-EDX instrument for analysis. The morphology of the samples was observed at magnification of $\times 2$ kV and 10 kV and the potential difference of 15 kV was used throughout the analysis. Three different spots of a sample were tested with EDX to study the local composition of the spots and to acquire the average composition for that sample.



Figure 3.3: Hitachi S-3400N SEM-EDX Instrument.

3.4.2 X-ray Diffractometer (XRD)

Shimadzu Diffractometer 6000 model of XRD was utilized to acquire XRD patterns for each MOF samples in order to identify each sample. Prior to the analysis, the samples had to be prepared by compressing the sample powders into the aluminium sample holder. During the test, Cu-K α radiation ($\lambda = 1.540562 \text{ \AA}$) radiation was focused onto the sample at ambient temperature. The MOF samples were scanned starting at 5 degree to set degree at the scan rate of 1.2 degree per minute.



Figure 3.4: Shimadzu Diffractometer 6000 model of XRD.

3.4.3 Fourier-Transform Infrared Spectrometer (FTIR)

The FTIR model that was being utilized during the study was Nicolet iS10. It is an analytical equipment used to identify functional group in organic and polymeric sample. Prior to the test, the sample holder and the detector probe had to be cleaned with diluted alcohol. After that, put a small amount of the sample on top of the sample holder and tightened up the screw until first click sound then only can start the analysis. Each sample was subjected to 16 scans from wavenumbers range from 4000 cm^{-1} to 400 cm^{-1} with an interval of 1 cm^{-1} and at the resolution of 4 cm^{-1} .



Figure 3.5: Nicolet iS10 FTIR Spectroscopy.

3.5 Carbon Dioxide (CO₂) Gas Adsorption Test

The experimental set up for measuring the CO₂ gas adsorption of the fabricated MOFs is shown in Figure 3.6. Prior to the test, the mass of the MOF was weighed by using a precision weight balance. Subsequently, the MOF was inserted into a tightly seal porous bag and the weight of the MOF with the gas was measured. Later, the porous bag with MOFs was inserted into a stainless-steel vessel for gas permeation study.

Subsequently, pure CO₂ gas was purged into the vessel for a predetermine sampling time of 20 minutes (Figure 3.7). Throughout the gas adsorption test, pressure inside the vessel was kept constant atmospheric pressure, which could be observed from a pressure gauge. Upon the completion of the gas adsorption test, the final weight of the MOFs is re-measured. The CO₂ gas adsorption capacity for this type of MOFs was then can be calculated from the difference of final and initial weight of the MOFs.

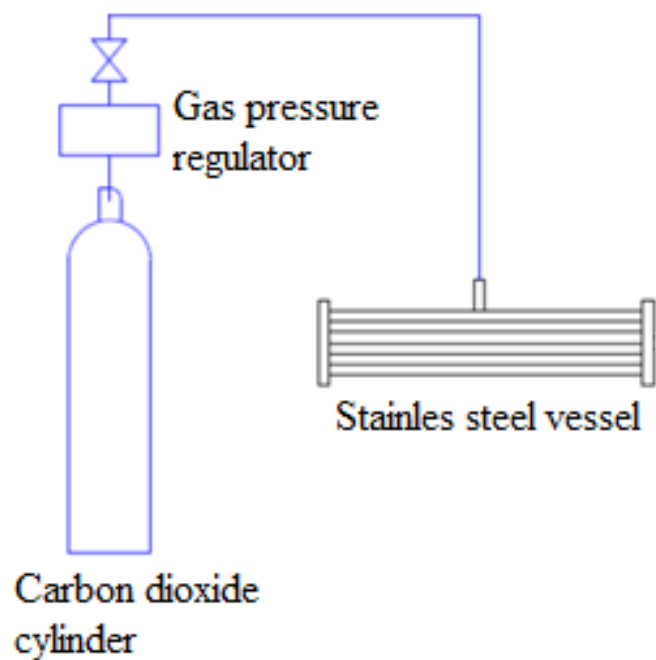


Figure 3.6: Gas Adsorption Test Setup.

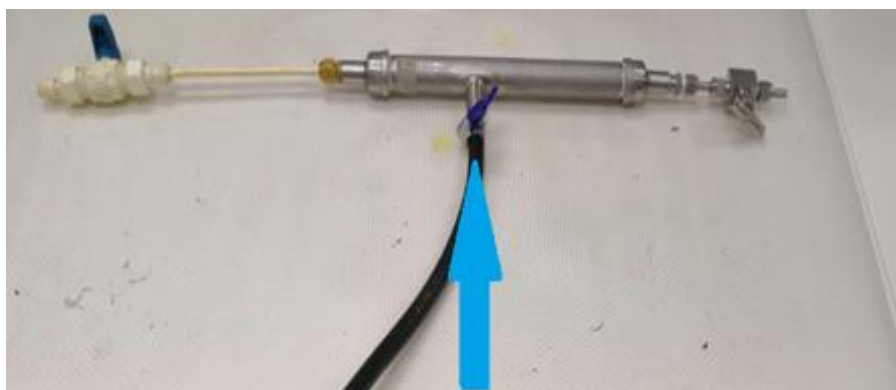


Figure 3.7: Stainless Steel Closed Vessel (Blue Arrow Indicates the CO₂ Gas Flow).

CHAPTER 4

RESULTS AND DISCUSSION

4.1 Morphological Studies

4.1.1 For MIL-101(Cr) Study

The raw Chromium (III) Nitrate Nonahydrate, $\text{Cr}(\text{NO}_3)_3 \cdot 9\text{H}_2\text{O}$ was present dark purple colour while 1,4-benzene dicarboxylic acid (BDC) was in white colour. The colour of the mixture turned into grey colour after grinding them together according to predetermined molar ratio by using mortar and pestle. Subsequently, the mixture was put into oven and heating at 220°C for predefined duration. The product (MIL-101 (Cr)) appeared in green. Figure 4.1 shows how the colour of the sample changed along the synthetic route for this type of MOF powder.

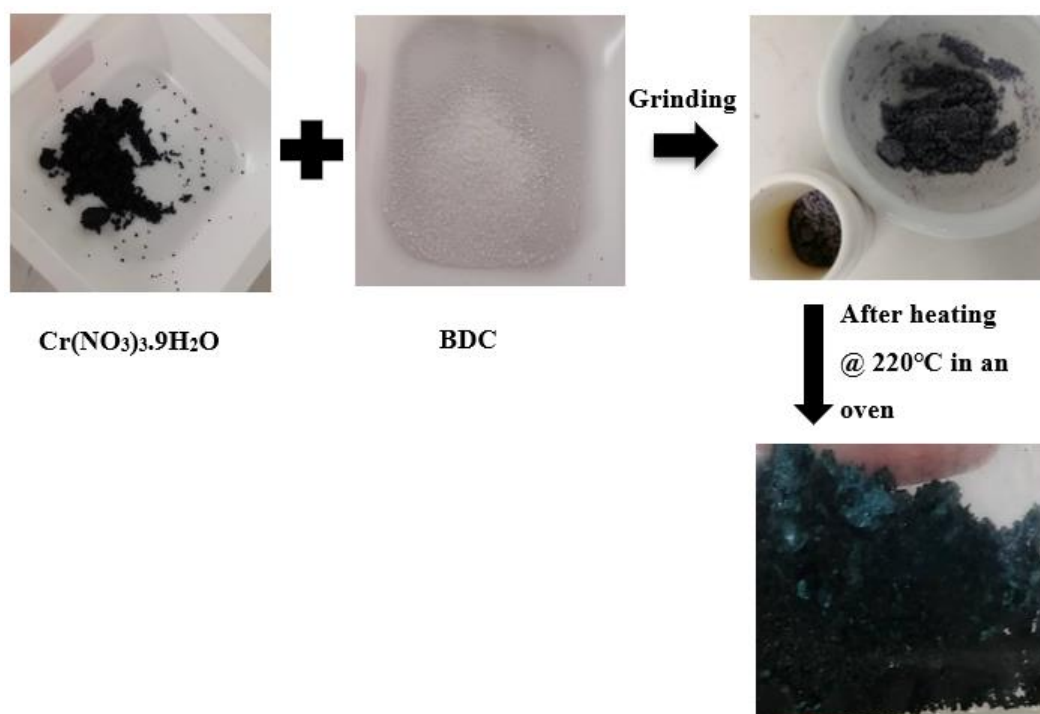


Figure 4.1: Colour Changes Along the Synthesis Process for MIL-101 (Cr).

4.1.2 For UiO-66(Ce) Study

Raw Cerium Ammonium Nitrate (CAN) powder was in dark orange colour, whereas BDC (terephthalic acid) was in the form of white powder. After grinding them together at predetermined molar ratio by using mortar and pestle, the powder mixture

colour became yellow orange colour. After that, the powder mixture was placed in oven to be heated at 120 °C for 24 hours. The colour of the powder turned to darker yellow orange colour. After the last step by washing the samples with DMF solvent and Acetone by using centrifuge to eliminate any unreacted reagents, then only off-white colour Ce-UiO-66 product was recovered. Figure 4.2 shows the colour changes of the sample along the synthetic route for this type of MOF powder.

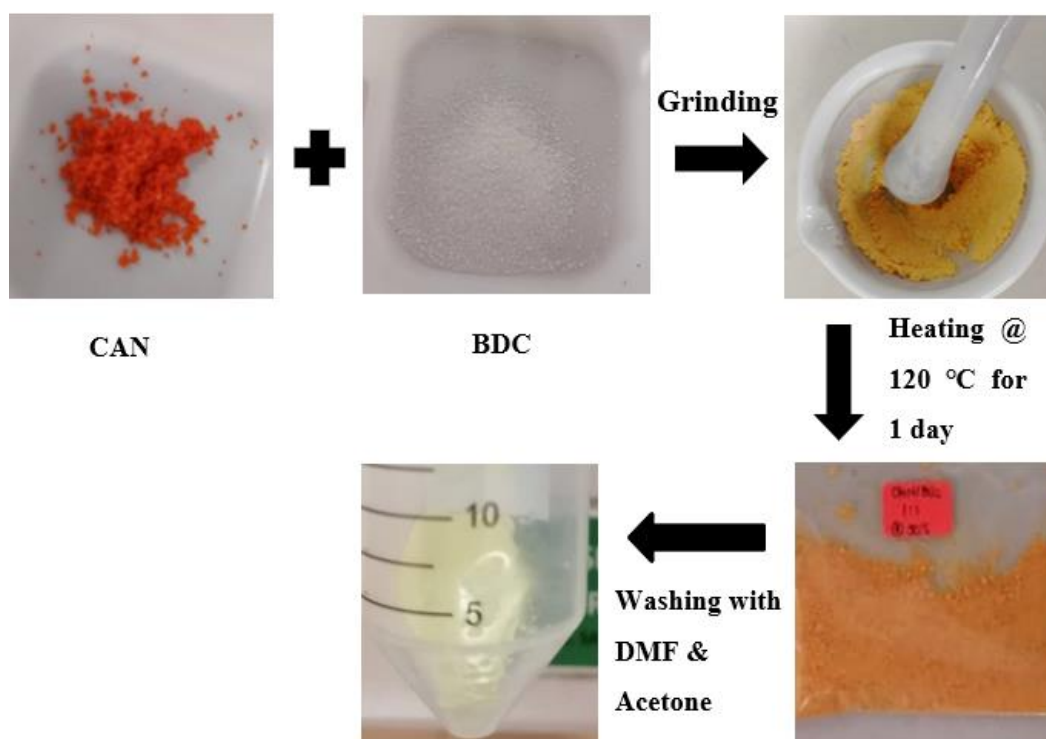


Figure 4.2: Colour Changes Along the Synthesis Process for UiO-66 (Ce).

4.2 X-Rays Diffraction (XRD) Graphs

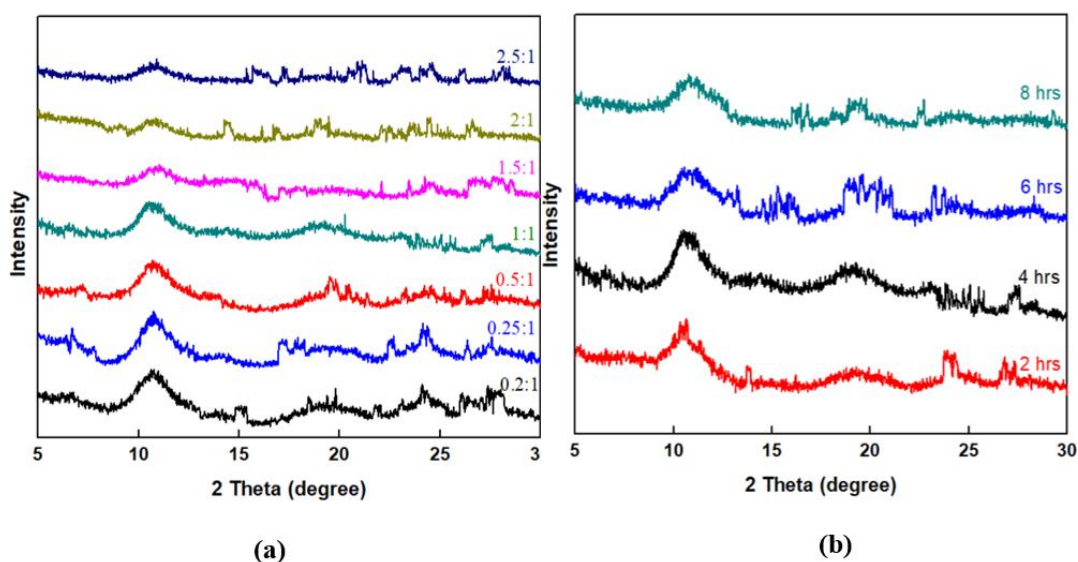


Figure 4.3: XRD Patterns of Various MIL-101 (Cr) Samples with (a) Different Cr/BDC Molar Ratio and (b) Different Crystallization Time.

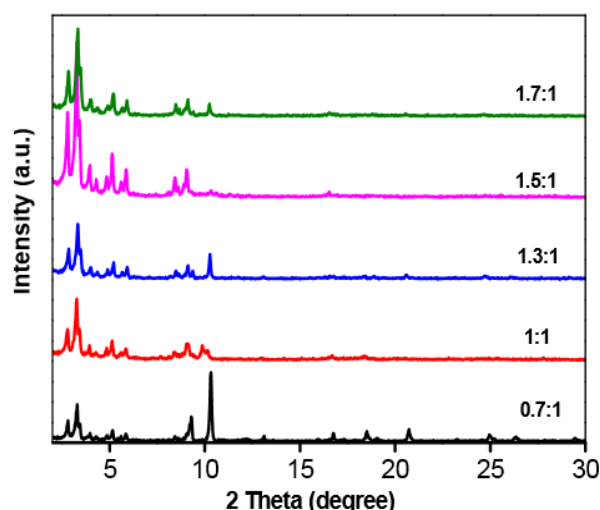


Figure 4.4: XRD Patterns of Various MIL-101 (Cr) Samples in Literature Review (Leng, et al., 2016).

Figure 4.4 shows the XRD pattern of MIL-101 (Cr) MOF reported by Xu and his co-workers (Leng, et al., 2016), there are two significant peaks occurred: the highest and most significant peak happened at 2θ of 3 degree while another milder peak happened at 2θ of 11 degree.

The MIL-101 (Cr) MOF samples were scanned from 2 theta of 5° to 30° under this study due to the limitation of the instrument. By comparing the XRD

patterns obtained from this study (Figure 4.3) with the one reported by Xu et al.(2016) (Figure 4.4), the peak of all MOF samples were in good agreement with the literature, especially the peaks at 2θ of 11° , confirming the formation of the pure crystalline MIL-101 (Cr) solids.

The XRD patterns of different Cr to BDC molar ratio samples were identical (Figure 4.3 (a)). No additional peak was observed, indicating that no other crystalline phase existed within the samples. In addition, their width of the diffraction peaks was observed to be different with the changes of molar ratio. It is interesting to note that as the molar ratio between the Cr/BDC increasing, the width of the diffraction peak became larger, suggesting that the crystal size of the sample with high Cr/BDC molar ratio might be smaller than that with the samples with lower Cr/BDC molar ratio.

XRD patterns of various MIL-101 (Cr) samples with different crystallization time as illustrated in Figure 4.3 (b). The peak patterns for these 4 different crystallization time samples were similar except the peak width for the sample with crystallization time of 2 hours appeared to be the smallest, suggesting its crystallite size is the largest.

4.3 Scanning Electron Microscopy (SEM) Images

4.3.1 Study on Cr/BDC Molar Ratio

The SEM images suggested different morphology for various MIL-101(Cr) samples that had been synthesized with different Cr to BDC molar ratio (Figure 4.6 to 4.12). The MIL-101 (Cr) is appeared to be an aggregation state of small particles with irregular granular shape with its particle sizing in approximate 40-200 nm as reported in literature studies (Leng, et al., 2016). However, due to the limitation on magnification scale of the available SEM instrument, the maximum magnification with good resolution image obtained was up to 10,000x magnification.

The SEM images for various molar ratio of MOF samples suggested that the particles size became larger as Cr/BDC molar ratio decreased, the surface roughness decreased accordingly as well. MOF sample with smaller particles size and higher surface roughness can perform better in carbon dioxide gas adsorption test as these features may have provided with greater surface area available for gas capture and storage. The SEM images for MIL-101(Cr)-2-4 (Figure 4.7) clearly shown that the sample was laid with many small round particles with particles size ranging from 1 μm to 3 μm in dimension. These regular round particles are believed to be the pure

chromium nanopowder (Figure 4.5) (NANOSHEL, 2015), revealing that high molar ratio of chromium element over the BDC organic ligand was used during the synthesis process would result in great amount of Cr starting element left with unreacted, lying on the surface of product sample, caused wastage on the initiating reagent.

The SEM image for MIL-101(Cr)-1.5-4 (Figure 4.8) displayed that the sample consisted of small irregular shaped particles, in which its morphology is different from the MIL-101(Cr)-2-4 sample, indicating that the crystal structure of MOF started to form as the Cr to BDC molar ratio decreased from 2:1 to 1.5:1. As the molar ratio was further decreased to 1 to 1, it can be clearly observed aggregate amount of small particles with irregular granular shape, suggesting MIL-101 (Cr) can grow nicely under the Cr/BDC molar ratio of 1 to 1.

However, by further reducing the molar ratio of Cr to BDC, it could be clearly observed from their SEM images that their particles sizes were growing bigger and their surface roughness were reducing. The SEM image for MIL-101 (Cr)-0.5-4, it composed of large particles with clean surface as compared to other samples (Figure 4.10). The reason for this phenomenon was believed to be the insufficient proportion of Cr metal centres in the reaction mixture is unable to drive the formation of MOF framework. Hence, the proper manipulation on the molar ratio of the starting materials, organic ligand and metal precursor are required to successfully synthesize the MOF sample with desired framework structure.

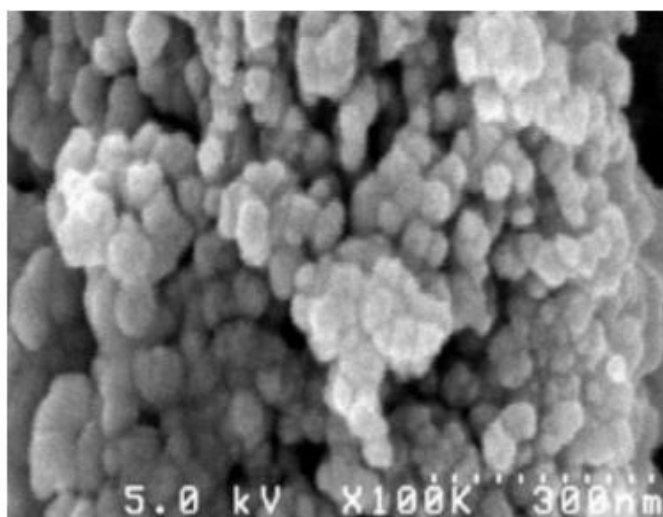


Figure 4.5: SEM Image for Pure Chromium Nanopowder (NANOSHEL, 2015).

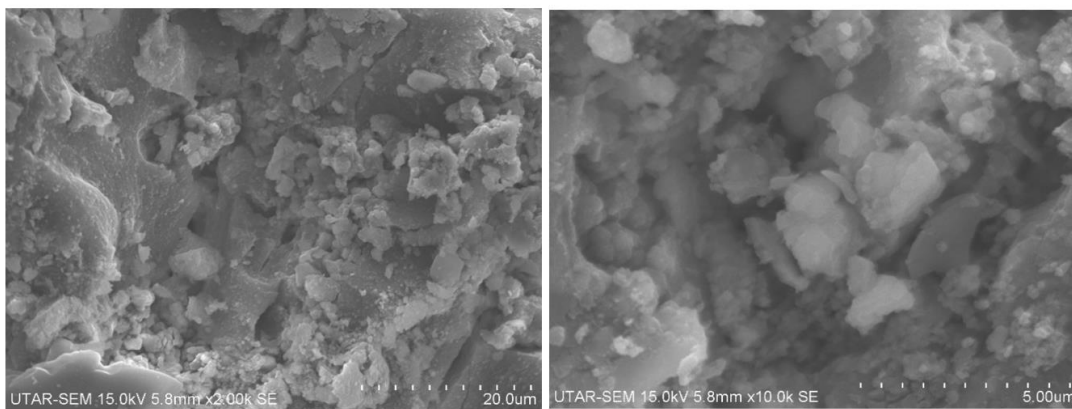


Figure 4.6: SEM Micrographs of MIL-101(Cr)-2.5-4.

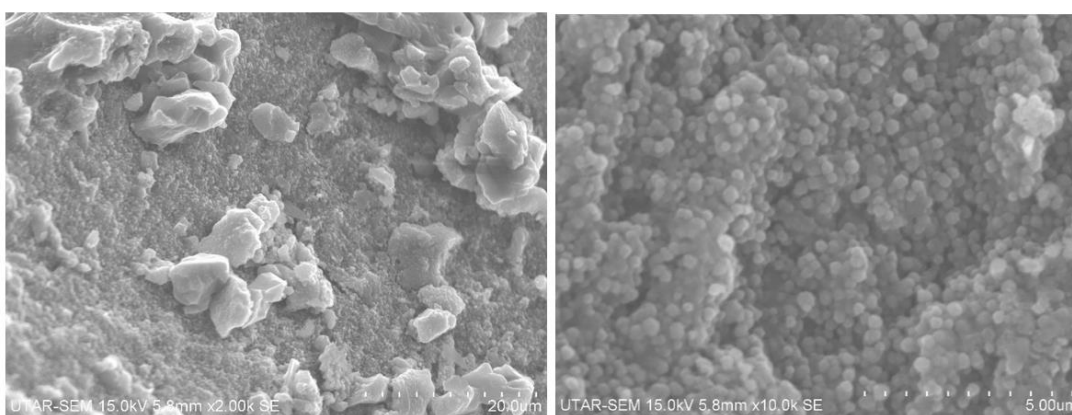


Figure 4.7: SEM Micrographs of MIL-101(Cr)-2-4.

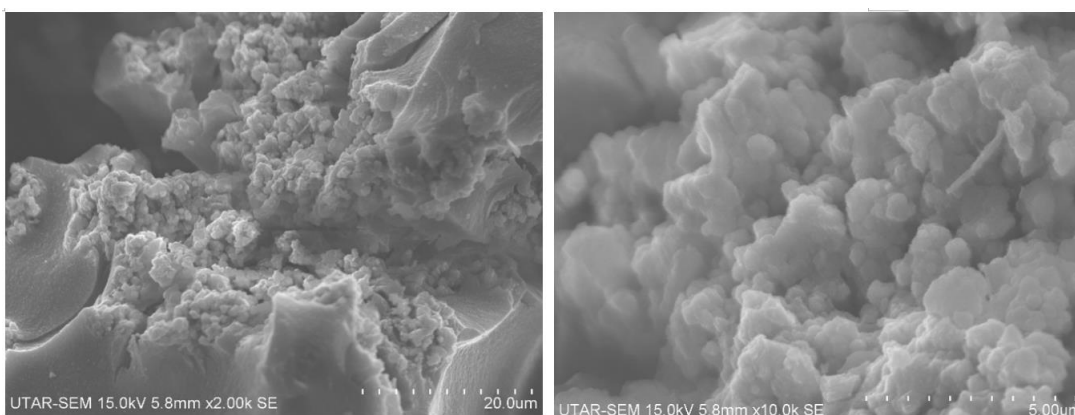


Figure 4.8: SEM Micrographs of MIL-101(Cr)-1.5-4.

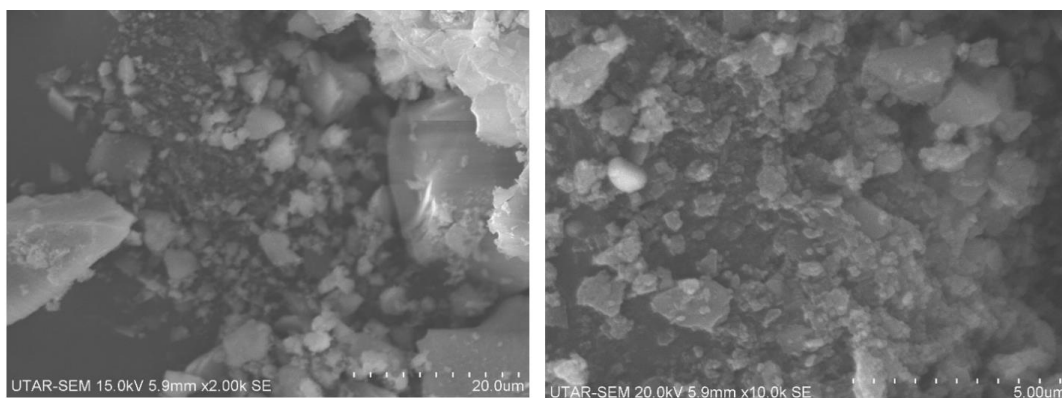


Figure 4.9: SEM Micrographs of MIL-101(Cr)-1-4.

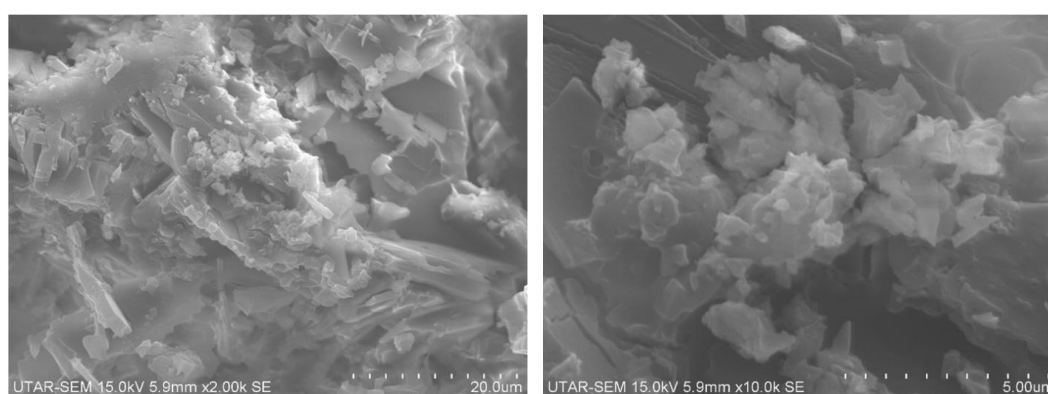


Figure 4.10: SEM Micrographs of MIL-101(Cr)-0.5-4.

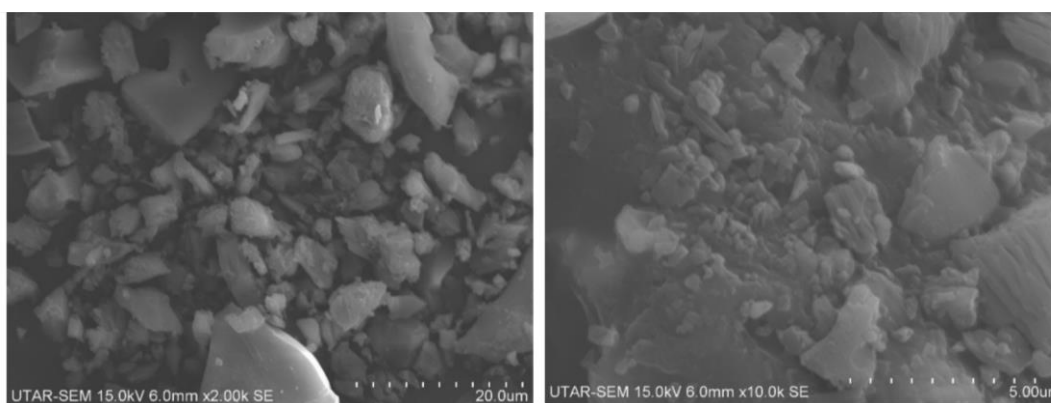


Figure 4.11: SEM Micrographs of MIL-101(Cr)-0.25-4.

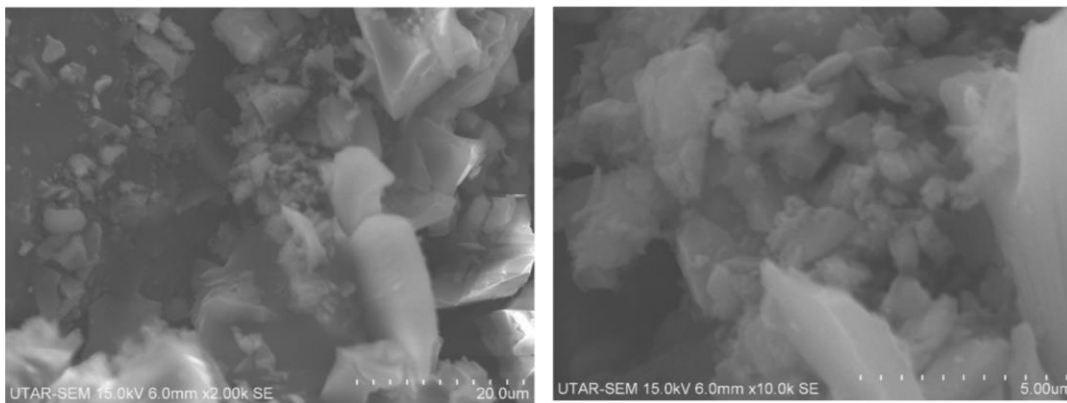


Figure 4.12: SEM Micrographs of MIL-101(Cr)-0.2-4.

4.3.2 Study on Crystallization Time

The SEM image of MIL-101(Cr)-1-2 (Figure 4.13), it showed a relatively clean and smooth surface. It is suggested that crystallization period of 2 hours is inadequate for the formation of MOF product. As the crystallization time increased to 4 hours, small particles with irregular granular shape can be observed (Figure 4.14) indicates the successfully formation of MIL-101(Cr) product. However, by further increasing the crystallization period, it could be observed from the SEM images (Figure 4.15 and Figure 4.16) that the particles aggregate together, thus causing their surface roughness reduced.

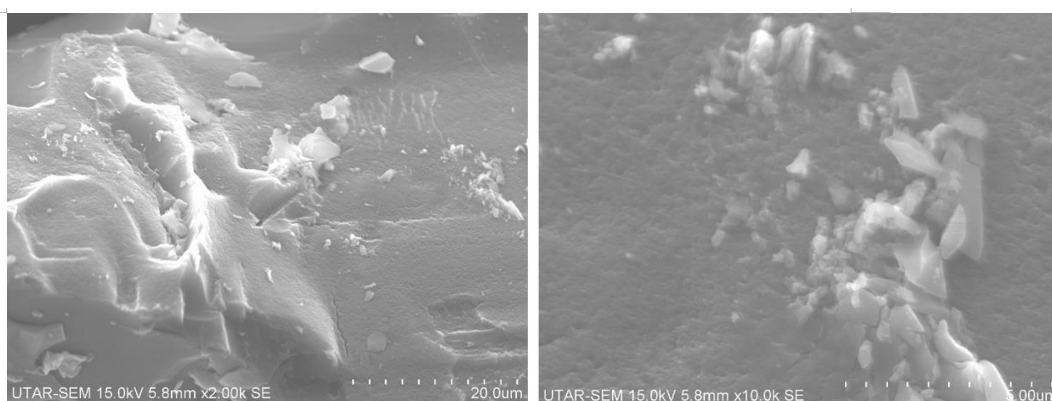


Figure 4.13: SEM Micrographs of MIL-101(Cr)-1-2.

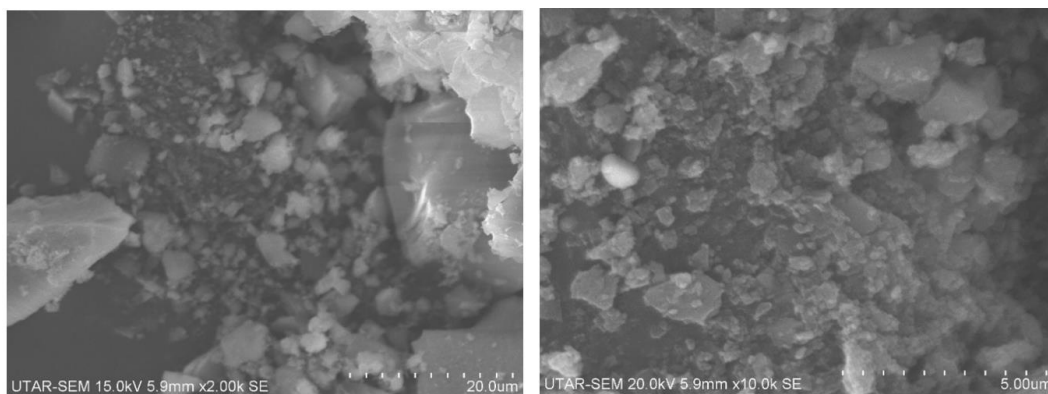


Figure 4.14: SEM Micrographs of MIL-101(Cr)-1-4.

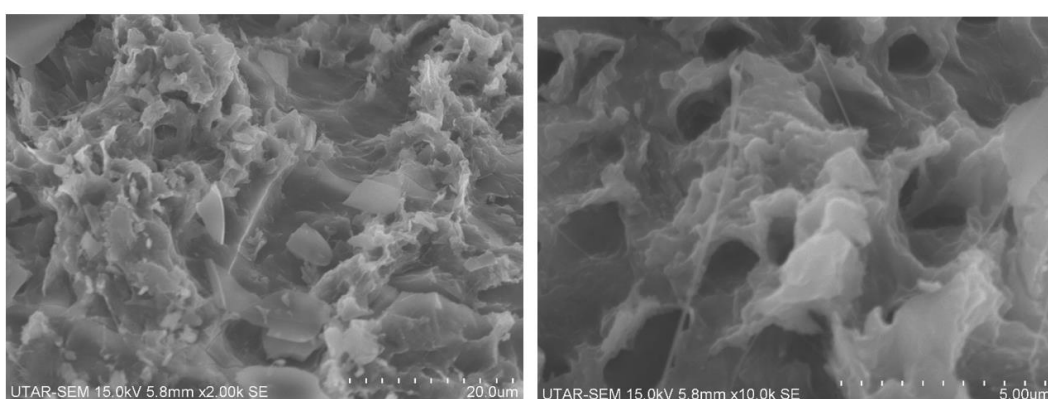


Figure 4.15: SEM Micrographs of MIL-101(Cr)-1-6.

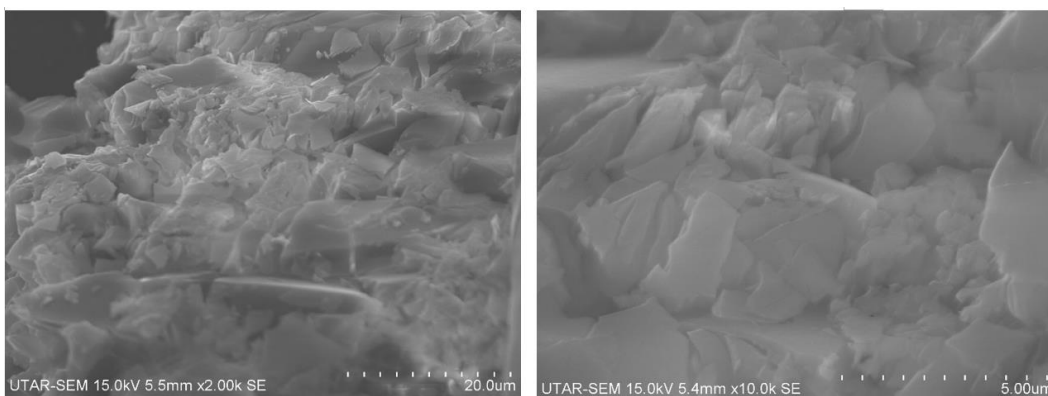


Figure 4.16: SEM Micrographs of MIL-101(Cr)-1-8.

4.4 Elemental Dispersive X-Rays (EDX) Results

Under this study, EDX analysis was employed to find out the elemental compositions of the samples that are successfully fabricated. Three elemental composition readings were taken from three different spots within a sample to get an average

reading with the aim of obtaining more reliable information regarding the elemental composition.

The EDX analysis result revealed that the Cr element was successfully incorporated into all the fabricated MIL-101 (Cr) samples. Carboxylic organic linker that participated the reaction was the source for the existence of C atom and O atom within the samples.

Theoretically, the weight percentage of Cr element should increase as the use of molar ratio between the Cr and BDC increased during the synthesis of samples (Leng, et al., 2016). However, as seen in Table 4.1, the Cr atom weight percentage for MIL-101(Cr)-0.5-4 was smaller than that of MIL-101(Cr)-0.25-4, which did not satisfy the theory. It is believed that the Cr element was not well-incorporated within the MIL-101(Cr)-0.5-4 sample. However, as overall result, the result was in accordance with the theoretical correlation stated in above.

Table 4.1: Elemental Composition of MIL-101 (Cr) with Different Cr/BDC Molar Ratio.

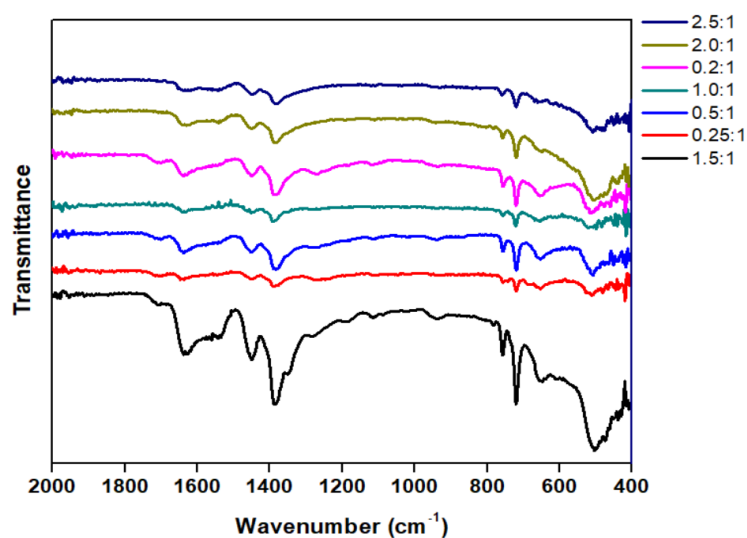
Sample	C (wt%)	O(wt%)	Cr(wt%)
MIL-101(Cr)-0.2-4	42.74	33.05	24.22
MIL-101(Cr)-0.25-4	40.73	32.99	26.28
MIL-101(Cr)-0.5-4	45.79	32.21	22.01
MIL-101(Cr)-1-4	41.45	31.02	27.52
MIL-101(Cr)-1.5-4	37.83	33.07	29.10
MIL-101(Cr)-2-4	29.52	37.41	33.07
MIL-101(Cr)-2.5-4	30.05	34.69	35.27

Table 4.2 shows the EDX analysis result for MIL-101 (Cr) samples fabricated with different crystallization time. There was no noteworthy correlation between the crystallization time and the Cr atom weight percentage. Sample with crystallization time of 8 hours had been incorporated with the highest weight percentage of Cr atom while the sample with crystallization time of 6 hours has the least Cr element weight percentage. However, quite satisfactory amount of Cr atom was able to be incorporated within the MIL-101(Cr) samples as overall.

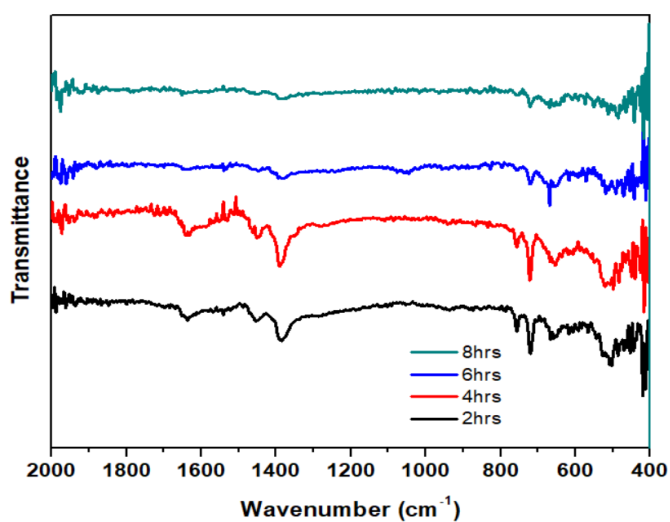
Table 4.2: Elemental Composition of MIL-101 (Cr) with Different Crystallization Time.

Sample	C (wt%)	O (wt%)	Cr (wt%)
MIL-101(Cr)-1-2	31.76	36.30	31.94
MIL-101(Cr)-1-4	41.45	31.02	27.52
MIL-101(Cr)-1-6	41.27	36.24	22.49
MIL-101(Cr)-1-8	30.30	34.60	35.09

4.5 FTIR Analysis



(a)



(b)

Figure 4.17: FTIR Spectra of Various MIL-101 (Cr) Samples with (a) Different Cr/BDC Molar Ratio and (b) Different Crystallization Time.

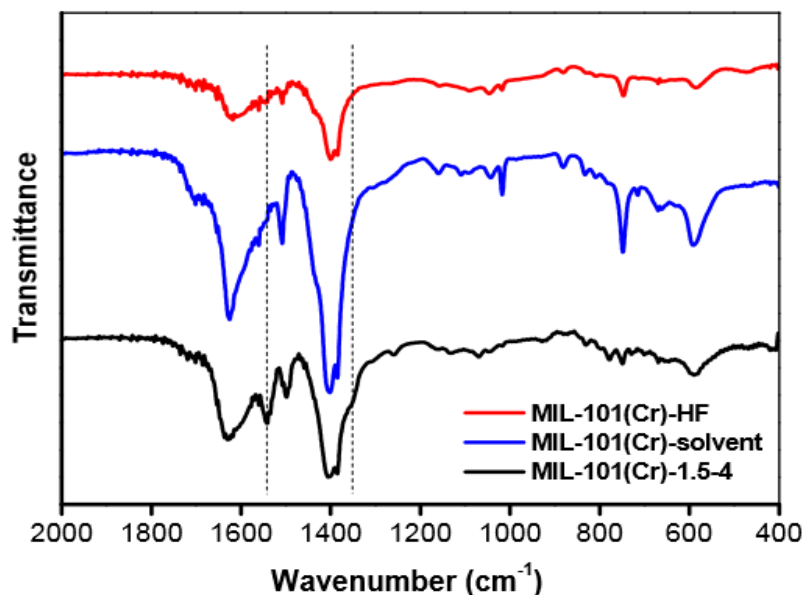


Figure 4.18: FTIR Spectra of Various MIL-101 (Cr) MOF samples (Leng, et al., 2016).

The region from 1200 cm^{-1} to 700 cm^{-1} in the infrared spectrum is called as the fingerprint region. Large number of bonds can be found in this region, including of C-O, C-C and C-N single bond stretches, C-H bending vibrations and some benzene rings bands. The function for this fingerprint region is to provide a fingerprint for a sample (libraries, 2019). The FTIR spectra of the synthesized MIL-101 (Cr) samples were well corresponding with that reported in the literature (Figure 4.18), especially for the fingerprint region. Hence, this confirming the formation of MIL-101 (Cr) MOF. An intense absorption band is observed at 1390 cm^{-1} due to symmetric (O-C-O) vibration of the benzene ring. While the moderate intensity of absorption band observed at wavenumber of 720 cm^{-1} is attributed to mono-substituted benzene ring (Figure 4.17) (Huang, et al., 2018). The FTIR spectra of MIL-101 (Cr) samples with different Cr/BDC molar ratio and crystallization time were similar in terms of peak shape and location of peak.

4.6 Results for Gas Adsorption Test

All the fabricated MOF samples were conducted the gas adsorption test in order to investigate their CO_2 gas uptake and storage performance. This gas adsorption test was carried out at room temperature and atmospheric pressure. During the test, MOF sample placed onto the teabag would be surrounded with pure CO_2 gas flow for the

sample to adsorb the CO₂ gas to its maximum within the predetermined duration of time. The result for the CO₂ gas adsorption capacity were expressed in term of mmol of CO₂ gas per gram of sample under this research study.

The CO₂ gas adsorption results for MIL-101 (Cr) samples with different Cr/BDC molar ratio were presented in Table 4.3 and Figure 4.19. Starting from the lowest Cr/BDC molar ratio sample, its CO₂ gas adsorption capacity is 8.0847 mmol/g. As the Cr/BDC increased from 0.2:1 to 1:1, the adsorption capacity increased as well correspondingly. Sample with Cr to BDC molar ratio of 1 to 1 achieved the highest adsorption capacity of, 18.7772 mmol/g among all the tested molar ratios. By further increasing the molar ratio, the adsorption capacity dropped in responding. Besides, Cr/BDC molar ratio of 1.5 to 1 and 0.5 to 1 have comparably high carbon dioxide gas adsorption capacity, 18.0378 mmol/g and 18.0037 mmol/g respectively.

Among of these seven MIL-101 (Cr) samples with different molar ratios, Cr to BDC molar ratio of 2.5 to 1 sample exhibited the lowest adsorption capacity to carbon dioxide gas, which is only 1.2321 mmol/g. As the overall result, the gap between the highest and the lowest adsorption capacity towards CO₂ gas were obvious, indicating that the molar ratio between the Cr atom to the BDC may have great influence towards the samples' CO₂ gas adsorption properties. Since the MIL-101(Cr)-1-4 sample has the highest CO₂ gas uptake capacity as compared to the other molar ratios, it could be concluded that the Cr/BDC molar ratio of 1:1 can produce the MIL-101(Cr) MOF with fairly good CO₂ gas adsorption performance.

While for the MIL-101(Cr) samples with different crystallization time, they could not be tested their CO₂ gas adsorption capacity due to the implementation of MCO that caused the cancellation of CO₂ gas adsorption test slot. Hence, the CO₂ gas adsorption result analysis for studying the effect of crystallization time towards the samples' gas adsorption capacity was unable to be performed.

Table 4.3: Carbon Dioxide Gas Adsorption Result for MIL-101 (Cr) Samples with Different Molar Ratio of Cr to BDC.

Cr/BDC (mol)	Weight before test (grams)	Weight after test (grams)	Weight difference/CO ₂ gas adsorbed (grams)	Moles of CO ₂ gas adsorbed (mmol)	CO ₂ gas adsorption capacity (mmol/g)
2.5:1	1.3170	1.3884	0.0714	1.6227	1.2321
2:1	1.4295	2.0210	0.5915	13.4432	9.4041
1.5:1	0.9223	1.6543	0.7320	16.6364	18.0379
1:1	0.9039	1.6507	0.7468	16.9727	18.7772
0.5:1	0.9185	1.6461	0.7276	16.5364	18.0037
0.25:1	0.9075	1.3252	0.4177	9.4932	10.4608
0.2:1	1.0910	1.4791	0.3881	8.8204	8.0847

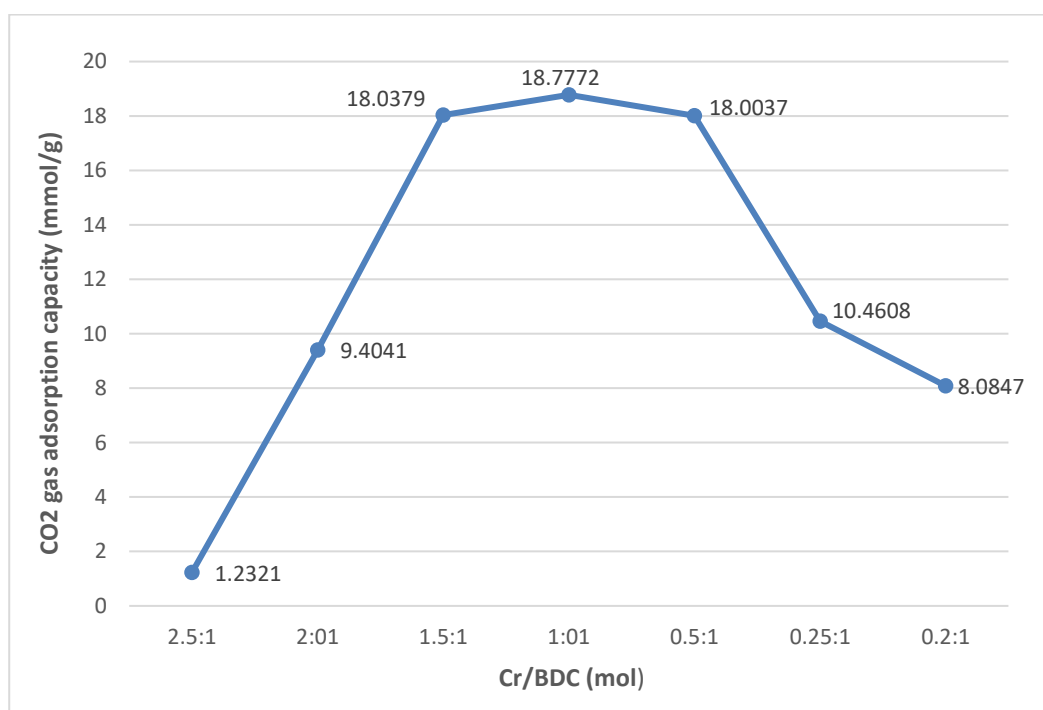


Figure 4.19: Carbon Dioxide Gas Adsorption Performance for MIL-101 (Cr) Samples with Different Molar Ratio of Cr to BDC.

CHAPTER 5

CONCLUSIONS AND RECOMMENDATIONS

5.1 Conclusions

In summary, MIL-101 (Cr) and UiO-66 (Ce) samples were successfully synthesized by solid phase reaction without the addition of solvent and HF (mechanochemical method). Their physical and chemical properties were characterized by various instrumental analyses.

XRD results indicated that the fabricated MIL-101 (Cr) MOFs were well agreed with the literature studies with the similar 2θ peak observed in the analysis. In general, the MIL-101 (Cr) MOF illustrated the dispersion of small irregular granular shaped particles. The MIL-101 (Cr) MOF with the Cr/BDC molar ratio of 1 to 1 (MIL-101(Cr)-1-4) exhibit the fine growth of irregular granular, suggested it yielding a greater surface area to volume ratio. The EDX analysis result revealed that the Cr element was successfully incorporated into all the fabricated MIL-101 (Cr) MOF in regardless of the loading of organic acid and crystallization time. The FTIR spectra of the synthesized MIL-101 (Cr) MOFs suggested the spectrum are well corresponding with that reported in the literature, especially for the fingerprint region. Hence, this confirming the formation of MIL-101 (Cr) MOF. The CO₂ gas adsorption result exhibited that the MIL-101(Cr)-1-4 yield the highest adsorption capacity at 18.7772 mmol/g. The result from the gas adsorption study suggested that the MIL-101(Cr)-1-4 sample with the Cr/BDC molar ratio of 1:1 and crystallization time exhibits good CO₂ gas adsorption performance.

It can be concluded that optimization of synthetic parameters including the crystallization time, loading of organic acid and modulator is necessary to produce MOF samples with good CO₂ gas adsorption performance. In addition, due to the simplification, speed and environmental safety of the synthetic procedures of mechanochemical method, it will be of great significance for potential applications.

5.2 Recommendations for future work

Under this study, the physical and chemical properties along with the carbon dioxide gas adsorption performance for MIL-101 (Cr) samples had been studied and

performed. In contrast for UiO-66 (Ce) samples, their characterization test, including the SEM, EDX, XRD and FTIR together with the gas adsorption test had not been conducted due to the unpredicted cancellation of analysis slot that was caused by the implementation of Movement Control Order (MCO) in Malaysia.

Furthermore, the TGA analysis that was planned to conduct for both MIL-101 (Cr) and UiO-66 (Ce) samples to study their thermal stability had been cancelled as well due to the reason stated above. Hence, this unpredicted condition has limited the study on the relationship between the carbon dioxide gas adsorption performance and the physical and chemical properties of the samples and thus affect the completeness of this research study.

Therefore, it is recommended that comprehensive characterization instrumental analysis have to be conducted in order to optimize the gas adsorption performance of the MOF samples in future work.

Besides, based on the available results that have been obtained under this study, it is proved that the synthetic parameters play significant role in determining the CO₂ gas adsorption capability of MOF samples. Therefore, it is well recommended that different synthetic parameters other than the molar ratio of reactants and crystallization time can be manipulated to study their effects towards the MOF samples' CO₂ gas adsorption properties. Furthermore, mechanochemical synthetic method for MOF has great potential and hence it is advised to further develop this solvent-free method in synthesizing more different types of MOFs in future work.

REFERENCES

- Alhamami, M., Doan, H. and Cheng, C., 2014. A Review on Breathing Behaviors of Metal-Organic-Frameworks (MOFs) for Gas Adsorption. *National Center for Biotechnology Information, U.S. National Library of Medicine*, 7(4), p. 3198–3250.
- Bernini, M.C., Brusau, E.V., Narda, G.E., Echeverria, G.E., Pozzi, C.G., Punte, G. and Lehmann, C.W., 2007. The Effect of Hydrothermal and Non-Hydrothermal Synthesis on the Formation of Holmium(III) Succinate Hydrate Frameworks.. *European Journal of Inorganic Chemistry*, (5), pp. 684-693.
- Bhattacharjee, S., Chen, C. & Ahn, W.-S., 2014. Chromium terephthalate metal-organic framework MIL-101: synthesis, functionalization, and applications for adsorption and catalysis. *RSC Advances*, 4(94), p. 52500–52525.
- Bigdeli, M. and Morsali, A., 2015. Sonochemical synthesis of a nano-structured zinc(II) amidic pillar metal-organic framework. *Ultrasonics Sonochemistry*, 27, pp. 416-422.
- Bo, Q.B., Pang, J.J., Wang, H.Y., Fan, C.H. and Zhang, Z.W., 2015. Hydrothermal synthesis, characterization and photoluminescent properties of the microporous metal organic frameworks with 1,3-propanediaminetetraacetate ligand and its auxiliary ligand.. *Inorganica Chimica Acta*, 428 (0), pp. 170-175.
- Campanelli, M. et al., 2019. Solvent-Free Synthetic Route for Cerium(IV) Metal-Organic Frameworks with UiO-66 Architecture and Their Photocatalytic Applications. *ACS Publications*, 48(11), pp. 45031-45037.
- Carlos, A.O., Fauston, F.S., Malvestiti, I., Valeria, R.M., Dutra, J.D., Nivan, C.J., Ricardo, O.F. and Severino, A.J., 2013. Effect of temperature on formation of two new lanthanide metal-organic frameworks: Synthesis, characterization and theoretical studies of Tm(III)-succinate. *Journal of Solid State Chemistry*, 197(0), pp. 7-13.
- Carson, C., Brown, A., Sholl, D. and Nair, S., 2011. Sonochemical Synthesis and Characterization of Submicrometer Crystals of the Metal-Organic Framework Cu[(hfipbb)(H₂hfipbb)_{0.5}]. *Crystal Growth & Design*, 10(4505-4510), p. 11.
- Caskey, S., Wong-Foy, A. and Matzger, A., 2008. Dramatic tuning of carbon dioxide uptake via metal substitution in a coordination polymer with cylindrical pores. *J. Am. Chem. Soc.*, 130, p. 10870–10871.
- Coninck, H., Stephens, J. and Metz, B., 2009. Global learning on carbon capture and storage: A call for strong international cooperation on CCS demonstration. *Energy Policy*, 37, pp. 2161-2165.
- Dinda, S., 2013. Development of solid adsorbent for carbon dioxide capture from flue gas.. *Technol*, 109, pp. 64-71.

Dutrow, B. and Clark, C., 2019. *X-ray Powder Diffraction (XRD)*. [Online] Available at: https://serc.carleton.edu/research_education/geochemsheets/techniques/XRD.html [Accessed 27 July 2019].

Huang, X. et al., 2018. Adsorption characteristics of metal–organic framework MIL-101(Cr) towards sulfamethoxazole and its persulfate oxidation regeneration. *RSC Advances*, 8(49), pp. 27623-27630.

What's Your Impact, 2018. *Main sources of carbon dioxide emissions*. [Online] Available at: <https://whatsyourimpact.org/greenhouse-gases/carbon-dioxide-emissions> [Accessed 15 June 2019].

Islamoglu, T. et al., 2017. Cerium(IV) vs Zirconium(IV) Based Metal–Organic Frameworks for Detoxification of a Nerve Agent. *ACS Publication*, 29(7), pp. 2672-2675.

Jiang, H.L., Liu, B., Lan, Y.Q., Kuratani, K., Akita, T., Shioyama, H., Zong, F.Q. and Xu, Q., 2011. From metal-organic framework to nanoporous carbon: toward a very high surface area and hydrogen uptake.. *J Am Chem Soc.*, 133(31).

Joaristi, A.M., Alcaniz, J.J., Crespo, P.S., Kapteijin, F. and Gascon, J., 2012. Electrochemical Synthesis of Some Archetypical Zn²⁺, Cu²⁺, and Al³⁺ Metal Organic Framework. *Crystal Growth & Design*, 12(7), pp. 3489-3498.

Kaithwas, A., Prasad, A. and Verma, S., 2012. Industrial wastes derived solid adsorbents for CO₂ capture: A mini review. *Chem. Eng. Res. Design*, 90, pp. 1632-1641.

Karizi, F. Z., Safarifard, S. K. and Morsali, A., 2015. Ultrasound-assisted synthesis of nano-structured 3D zinc(II) metal–organic polymer: Precursor for the fabrication of ZnO nano-structure. *Ultrasonics Sonochemistry*, 23(0), pp. 238-245.

Kenji, S., 2011. *American Chemical Society*, 112, pp. 724-774.

Kitagawa, S., Kitaura, R. and Noro, S., 2004. Functional porous coordination polymers.. *Angew. Chem. Int. Ed.*, 42, p. 2334–2375.

Kızılel, S. and Keskin, S., 2011. Biomedical Applications of Metal Organic Frameworks. *2011 American Chemical Society*, 50(4), pp. 1799-1812.

Klimakow, M., Klobes, P., Thünemann, A.F., Rademann, K. and Emmerling, F., 2010. Mechanochemical Synthesis of Metal–Organic Frameworks: A Fast and Facile Approach toward Quantitative Yields and High Specific Surface Areas.. *Chemistry of Materials*, 22(18), pp. 5216-5221.

Klinowski, J., Paz, F.A., Silva, P. and Rocha, J., 2011. Microwave-Assisted Synthesis of Metal-Organic Frameworks. *Dalton Transactions*, 40 (2), pp. 321-330.

RTI Laboratories, 2015. *FTIR Analysis*. [Online] Available at: <https://rtilab.com/techniques/ftir-analysis/> [Accessed 27 July 2019].

NASA's Jet Propulsion Laboratory, 2019. *Climate Change: How Do We Know?*. [Online] Available at: <https://climate.nasa.gov/evidence/> [Accessed 17 June 2019].

Laboratory, E. S. C. T. a. N. J. P., 2019. *The Effects of Climate Change*. [Online] Available at: <https://climate.nasa.gov/effects/> [Accessed 17 June 2019].

Lammert, M. et al., 2015. Cerium-based Metal Organic Frameworks with UiO-66 Architecture: Synthesis, Properties and Redox Catalytic Activity. *Chemical Communications*, 51(63), pp. 12578-12581.

Le Quéré, C., Andres, R.J., Boden, T., Conway, T., Houghton, R.A., House, J.I., Marland, G., Peters, G.P., van der Werf, G.R., Ahlström, A., Andrew, R.M., Bopp, L., Canadell, J.G., Ciais, P., Doney, S.C., Enright, C. and Friedlingstein, P., 2013. *The global carbon budget 1959–2011*. [Online] Available at: <https://doi.org/10.5194/essd-5-165-2013>, [Accessed 16 June 2019].

Lee, Y.R., Kim, J. and Ahn, W.S., 2013. Synthesis of metal-organic frameworks: A mini review. *Korean Journal of Chemical Engineering*, 30(9), p. 1667–1680.

Leng, K.Y., Sun, Y.Y., Li, X.L., Sun, S. and Xu, W., 2016. Rapid Synthesis of Metal–Organic Frameworks MIL-101(Cr) Without the Addition of Solvent and Hydrofluoric Acid. *Cryst. Growth Design*, (16), pp. 1168-1171.

Liang, W.B. and D'Alessandro, D.M., 2013. Microwave-assisted solvothermal synthesis of zirconium oxide based metal-organic frameworks.. *Chemical Communications*, 49(35), pp. 3706-3708.

LibreTexts libraries, 2019. *Infrared: Interpretation*. [Online] Available at: [https://chem.libretexts.org/Bookshelves/Physical_and_Theoretical_Chemistry_Textbook_Maps/Supplemental_Modules_\(Physical_and_Theoretical_Chemistry\)/Spectroscopy/Vibrational_Spectroscopy/Infrared_Spectroscopy/Infrared%3A_Interpretation](https://chem.libretexts.org/Bookshelves/Physical_and_Theoretical_Chemistry_Textbook_Maps/Supplemental_Modules_(Physical_and_Theoretical_Chemistry)/Spectroscopy/Vibrational_Spectroscopy/Infrared_Spectroscopy/Infrared%3A_Interpretation) [Accessed 23 February 2020].

Li, L., Lv, G.C., Wang, P., Liu, Q., Chen, K. and Sun, W.Y., 2013. pH-Dependent cobalt(ii) frameworks with mixed 3,3[prime or minute],5,5[prime or minute]-tetra(1H-imidazol-1-yl)-1,1[prime or minute]-biphenyl and 1,3,5-benzenetricarboxylate ligands: synthesis, structure and sorption property. *CrystEngComm*, 15(45), pp. 9537-9543.

- Li, L., Wang, S.Y., Chen, T.L., Sun, Z.H., Luo, J.H. and Hong, M.C., 2012 b. Solvent-Dependent Formation of Cd(II) Coordination Polymers Based on a C2-Symmetric Tricarboxylate Linker. *Cryst. Growth Des.*, 12(8), pp. 4109-4115.
- Luan, X.J., Cai, X.H., Wang, Y.Y., Li, D.S., Wang, C.J., Liu, P., Hu, H.M., Shi, Q.Z. and Peng, S.M., 2006. An Investigation of the Self-Assembly of Neutral, Interlaced, Triple-Stranded Molecular Braids. *Chem. Eur. J.*, (12), pp. 6281-6289.
- McKinlay, A.C., Morris, R.E., Horcajada, P., Ferey, G., Gref, R., Couvreur, P. and Serre, C., 2010. BioMOFs: metal-organic frameworks for biological and medical applications.. *Angew Chem Int Ed Engl.*, 49(36).
- Millward, A.R. and Yaghi, O.M., 2005. Metal–Organic Frameworks with Exceptionally High Capacity for Storage of Carbon Dioxide at Room Temperature. *J. Am. Chem. Soc.*, 127, pp. 17998-17999.
- Mondal, M.K., Balsora, H.K. and Varshney.P, 2012. Progress and trends in CO2 capture/separation technologies: A review. *Energy*, 46, pp. 431-441.
- Mulligan, J., Ellison, G. and Levin, K., 2018. *6 Ways to Remove Carbon Pollution from the Sky*. [Online] Available at: <https://www.wri.org/blog/2018/09/6-ways-remove-carbon-pollution-sky> [Accessed 20 June 2019].
- Murdock, C.R., Lu, Z. and Jenkins, D.M., 2013. Effects of solvation on the framework of a breathing copper MOF employing a semirigid linker. *Inorg. Chem.*, 42, p. 2182–2187.
- NANOSHEL, 2015. *Chromium Nanopowder*. [Online] Available at: <https://www.nanoshel.com/product/chromium-nanopowder> [Accessed 23 February 2020].
- Nanowerk, 2019. *What is a MOF (metal organic framework)?*. [Online] Available at: <https://www.nanowerk.com/mof-metal-organic-framework.php> [Accessed 20 June 2019].
- Noro, S., Kitagawa, S., Kondo, M. and Seki, K., 2000. A New, Methane Adsorbent, Porous Coordination Polymer. *Angew Chem Int Ed Engl.*, 39(12), pp. 2081-2084.
- Pachauri, R.K. and Reisinger, A., 2007. *Climate Change 2007: Synthesis Report*, s.l.: IPCC.
- Pachfule, P., Das, D., Poddar, P. and Banerjee, P., 2011. Solvothermal Synthesis, Structure, and Properties of Metal Organic Framework Isomers Derived from a Partially Fluorinated Link. *Crystal Growth & Design*, 11(4), pp. 1215-1222.
- Pettinari, C., Marchetti, M., Mosca, N., Tosi, G. and Drozdov, A., 2017. Application of Metal-organic Frameworks. *Polymer International*, 66(6), pp. 731-744.

Pilloni, M., Padella, F., Ennas, G., Lai, S., Bellusci, M., Rombi, E., Sini, F., Pentimalli, M., Delitala, C., Scano, A., Cabras, V. and Ferino, I., 2015. Liquid-assisted mechanochemical synthesis of an iron carboxylate Metal Organic Framework and its evaluation in diesel fuel desulfurization. *Microporous and Mesoporous Materials*, 213(0), pp. 14-21

Roser, Hannah and Max, 2019. *CO₂ and other Greenhouse Gas Emissions*. [Online] Available at: <https://ourworldindata.org/co2-and-other-greenhouse-gas-emissions> [Accessed 16 June 2019].

Scientific, Eurofins, 2018. *Thermogravimetric Analysis (TGA)*. [Online] Available at: <https://www.eag.com/techniques/phys-chem/thermal-analysis-tga/> [Accessed 27 July 2019].

Susan, S., 2017. *Scanning Electron Microscopy (SEM)*. [Online] Available at: https://serc.carleton.edu/research_education/geochemsheets/techniques/SEM.html [Accessed 27 July 2019].

Trickett, C.A., Helal, J., Maythalony, B.A., Yamani, Z.H., Cordova, K.E. and Yaghi, O.M., 2017. The chemistry of metal–organic frameworks for CO₂ capture, regeneration and conversion. *Macmillan Publishers Limited*, 2, pp. 1-16.

Vieth, Janiak, C. and Jana, K., 2010. MOFs, MILs and more: concepts, properties and applications for porous coordination networks (PCNs). *New Journal of chemistry*, 34(11), pp. 2366-2388.

Wu, Y.P., Li, D.S., Fu, F., Dong, W.W., Zhao, J., Zou, K. and Wang, Y.Y., 2011. Stoichiometry of N-Donor Ligand Mediated Assembly in the ZnII - Hfipbb System: From a 2-Fold Interpenetrating Pillared-Network to Unique (3, 4) - Connected Isomeric Nets. *Cryst. Growth Des*, 11, pp. 3850-3857.

Yakovenko, A. A., Wei, Z.W., Wreidt, M., Li, J.R., Halder, G.J. and Zhou, H.C., 2014. Study of Guest Molecules in Metal–Organic Frameworks by Powder X-ray Diffraction: Analysis of Difference Envelope Density. *Crystal Growth & Design*, 14(11), pp. 5397-5407.

Zhang, F., Liang, H., Zhang, L. and Zhang, X., 2011. Solid-State Thermolysis Preparation of Co₃O₄ Nano/Micro Superstructures From Metal-Organic Framework for Supercapacitors. *Electrochem. Sci*, (6), pp. 2943 - 2954.

Zhang, K.L., Hou, C.T., Song, J.J., Deng, Y., Li, L., Ng, S.W. and Diao, G.W., 2012. Temperature and auxiliary ligand-controlled supramolecular assembly in a series of Zn(ii)-organic frameworks: syntheses, structures and properties. *CrystEngComm*, 14(2), pp. 590-600.

Zhang, W.H., Wang, Y.Y., Lermontova, E.K., Yang, G.P., Liu, B., Jin, J.C., Dong, Z. and Shi, Q.Z., 2010 b. Interaction of 1,3-Adamantanediactic Acid (H₂ADA) and Ditopic Pyridyl Subunits with Cobalt Nitrate under Hydrothermal Conditions: pH

Influence, Crystal Structures, and Their Properties.. *Crystal Growth & Design*, 10(1), pp. 76-84.

Zhao, A., 2012. *Adsorptive removal of CO₂ by amine functionalized sorbents: Experimental and kinetics study*, s.l.: University of Alberta Libraries, Alberta, USA.

Zhao, D., Yuan, D. & Zhou, H., 2008. The current status of hydrogen storage in metal–organic frameworks. *Energy & Environmental Science*, (2), pp. 222-235.